Research Article
Experimental and Translational Hepatology

JOURNAL OF HEPATOLOGY

IL-10 dampens antitumor immunity and promotes liver metastasis via PD-L1 induction

Ahmad Mustafa Shiri[1,2,†], **Tao Zhang**[1,2,†], Tanja Bedke[1,2], Dimitra E. Zazara[3,4], Lilan Zhao[5], Jöran Lücke[1,2,5], Morsal Sabihi[1,2], Antonella Fazio[1,2], Siwen Zhang[1,2], Daniele V.F. Tauriello[6], Eduard Batlle[7,8,9], Babett Steglich[1,2], Jan Kempski[1,2,10], Theodora Agalioti[5], Mikołaj Nawrocki[1,2], Yang Xu[5], Kristoffer Riecken[11], Imke Liebold[1,2,12], Leonie Brockmann[1,2], Leonie Konczalla[5], Lidia Bosurgi[1,2,12], Baris Mercanoglu[5], Philipp Seeger[5], Natalie Küsters[5], Panagis M. Lykoudis[13,14], Asmus Heumann[5], Petra C. Arck[4], Boris Fehse[11], Philipp Busch[5], Rainer Grotelüschen[5], Oliver Mann[5], Jakob R. Izbicki[5], Thilo Hackert[5], Richard A. Flavell[15,16], Nicola Gagliani[1,2,5], Anastasios D. Giannou[1,2,5,*,‡], Samuel Huber[1,2,*,‡]

Journal of Hepatology **2024**. vol. 80 | 634–644

Check for updates

Background & Aims: The liver is one of the organs most commonly affected by metastasis. The presence of liver metastases has been reported to be responsible for an immunosuppressive microenvironment and diminished immunotherapy efficacy. Herein, we aimed to investigate the role of IL-10 in liver metastasis and to determine how its modulation could affect the efficacy of immunotherapy *in vivo*.

Methods: To induce spontaneous or forced liver metastasis in mice, murine cancer cells (MC38) or colon tumor organoids were injected into the cecum or the spleen, respectively. Mice with complete and cell type-specific deletion of IL-10 and IL-10 receptor alpha were used to identify the source and the target of IL-10 during metastasis formation. Programmed death ligand 1 (PD-L1)-deficient mice were used to test the role of this checkpoint. Flow cytometry was applied to characterize the regulation of PD-L1 by IL-10.

Results: We found that *Il10*-deficient mice and mice treated with IL-10 receptor alpha antibodies were protected against liver metastasis formation. Furthermore, by using IL-10 reporter mice, we demonstrated that Foxp3+ regulatory T cells (Tregs) were the major cellular source of IL-10 in liver metastatic sites. Accordingly, deletion of IL-10 in Tregs, but not in myeloid cells, led to reduced liver metastasis. Mechanistically, IL-10 acted on Tregs in an autocrine manner, thereby further amplifying IL-10 production. Furthermore, IL-10 acted on myeloid cells, *i.e.* monocytes, and induced the upregulation of the immune checkpoint protein PD-L1. Finally, the PD-L1/PD-1 axis attenuated CD8-dependent cytotoxicity against metastatic lesions.

Conclusions: Treg-derived IL-10 upregulates PD-L1 expression in monocytes, which in turn reduces CD8+ T-cell infiltration and related antitumor immunity in the context of colorectal cancer-derived liver metastases. These findings provide the basis for future monitoring and targeting of IL-10 in colorectal cancer-derived liver metastases.

Introduction

Liver metastasis is one of the major causes of cancer-associated mortality.[1] Among cancer entities, colorectal cancer (CRC) is one of the most common cancers worldwide with a high metastatic rate – mainly to the liver.[2] Furthermore, other entities like lung cancer, breast cancer, and skin cancer, metastasize to the liver.[3] Despite decades of cancer research, treating metastatic cancers still poses a challenge. Thus, further research focusing on metastasis formation and progression is essential. The presence of liver metastases can also influence the selection of appropriate therapeutic regimens, since it has been associated with reduced responsiveness to immune checkpoint inhibitors, for example, anti-programmed death 1 (PD-1) and anti-programmed death ligand 1 (PD-L1) antibodies.[4] The roles and regulation of immune checkpoints in liver metastases have not yet been well described. Interestingly, PD-L1 expression was found to be higher in liver metastases compared to primary CRC, while positively correlating with the number of infiltrating T cells.[5] Additionally, it was demonstrated that radiotherapy, specifically on the liver, could increase tumor-specific T-cell survival and restore immunotherapy efficacy.[4] Thus, it is critical to decipher the regulation of

Keywords: liver metastasis; IL-10; PD-L1; immunotherapy; immune cells.
Received 15 June 2023; received in revised form 12 December 2023; accepted 18 December 2023; available online 30 December 2023
* Corresponding authors. Addresses: Samuel Huber, M.D.; Section of Molecular Immunology and Gastroenterology, I. Department of Medicine, Center of Internal Medicine, University Medical Center Hamburg-Eppendorf, Martinistr. 52, 20246 Hamburg, Germany; Tel.: +49 40 57273, fax +49 40 7410 59038. (S. Huber), or Anastasios Giannou; Section of Molecular Immunology and Gastroenterology, I. Department of Medicine, Center of Internal Medicine and Department of General, Visceral and Thoracic Surgery, University Medical Center Hamburg-Eppendorf, Hamburg 20246, Germany; Tel.: +49 40 20980, fax +49 40 7410 59038 (A.D. Giannou).
E-mail addresses: s.huber@uke.de (S. Huber), a.giannou@uke.de (A.D. Giannou).
† These authors shared first authorship/contributed equally to this work
‡ These authors shared senior authorship/contributed equally to this work
https://doi.org/10.1016/j.jhep.2023.12.015

immune checkpoint molecules in liver metastasis to increase the effectiveness of immunotherapy.

IL-10, the founding member of the IL-10 cytokine family, is known as a key cytokine for immune regulation.[6] In the last decade, several studies analyzed the role of IL-10 in primary cancer.[7–10] IL-10 administration in preclinical models[8,9] and clinical trials[11,12] showed a beneficial effect on primary tumor sites, thereby identifying IL-10 as a new therapeutic approach for patients with different cancer entities. In fact, IL-10 seems to play a protective role in tumor immunology by increasing the survival and cytotoxicity of CD8+ T cells.[13] In line with this, IL-10 was reported to be similarly protective in lung metastases.[10] In contrast, the role of IL-10 in liver metastasis has so far been poorly described, with the exception of a recent *in vitro* study. In this study, organotypic slice cultures from human CRC-derived liver metastases were used and antitumor effects of a neutralizing antibody against IL-10 both alone as treatment and in combination with exogenously administered carcinoembryonic antigen-specific chimeric antigen receptor T (CAR-T) cells were analyzed. Interestingly, the authors found that IL-10 blockade could enhance the effectiveness of CAR-T cell treatment.[14] However, the cellular source of IL-10, its function and mechanism of action *in vivo* was not analyzed in this study. This was the aim of our work. Using several mouse models, we found that despite the protective effect on primary tumors, IL-10 instead promotes liver metastasis. IL-10 does not affect cancer cell extravasation, but rather influences later stages of the metastatic cascade. Specifically, Foxp3+Treg-derived IL-10 acts on Foxp3+Tregs themselves, thereby amplifying IL-10 production. Furthermore, IL-10 promotes PD-L1 upregulation on monocytes, which subsequently suppresses CD8+ T-cell-mediated immune surveillance. Accordingly, the deletion of PD-L1 resulted in a reduction of liver metastases. In conclusion, these data identify IL-10 as a pro-metastatic factor in liver metastasis formation and characterize this cytokine as a regulator of PD-L1.

Materials and methods

Mice

C57BL/6J, Il10$^{-/-}$, *Il10*$^{flox/flox}$*;Foxp3*$^{cre+}$, *Il10*$^{flox/flox}$*;Lysm*$^{cre+}$, *Rag*$^{-/-}$*(Yale), Il10*^{eGFP}*;Foxp3*^{RFP}, *Il10ra*$^{flox/flox}$*;Cdh5*$^{cre+}$, *Il17a*$^{cre+}$*;Rosa26*^{floxSTOPfloxYFP}*;Foxp3*^{RFP}, *Il10ra*$^{flox/flox}$*;Lysm*$^{cre+}$, *Il10ra*$^{flox/flox}$*;Cd11c*$^{cre+}$, *Il10ra*$^{flox/flox}$*;Il17a*$^{cre+}$, *DEREG, Pdl1*$^{-/-}$ were housed in the animal facility of the University Medical Center Hamburg-Eppendorf under specific pathogen-free conditions. *Il10ra*$^{flox/flox}$ mice (kindly provided by Richard A. Flavell) and *Il10*$^{flox/flox}$ were validated and characterized before.[15,16] Details of the sources of these mouse lines were listed in the supplementary CTAT table. Age- (8-14 weeks) and sex-matched littermates were used for experiments. All animal experiments were approved by the Institutional Review Board "Behörde für Justiz und Verbraucherschutz, Lebensmittelsicherheit und Veterinärwesen" (Hamburg, Germany).

Cancer cell lines and organoids

Lewis lung carcinoma (LLC) and colon adenocarcinoma (MC38) cancer cells were cultured in DMEM containing 10% FBS and penicillin-streptomycin. MC38 cells were lentivirally transduced to express the green fluorescence protein (MC38-GFP) and puromycin resistance. As an alternative neutral control, MC38 cells were lentivirally transduced to express a non-targeted short hairpin RNA (MC38-shC) and a puromycin resistance. Transduced MC38 were cultured with 10% FBS DMEM in the presence of penicillin-streptomycin and puromycin.[17] Lentiviral vectors were produced following our established protocols.[18] Cells were harvested at around 80% confluency for *in vivo* injections. Mouse tumor organoids 129 (MTO129) were kindly provided by Prof. Eduard Batlle. MTO culture was performed as previously described.[19]

Mouse models for liver metastasis induction

Spontaneous liver metastasis induction

Spontaneous liver metastasis was established by injecting cancer cells into the cecum (2×10^5 cells per mouse), as described previously.[20] The humane endpoint of mice was in accordance with the approved animal protocol. Mice were anesthetized with isoflurane and an incision was made in the middle of the abdomen to expose the cecum. This was followed by an orthotopic injection of cancer cells dissolved in 50 µl PBS into the cecum using a 32-G needle until a solid bubble was formed on the caecum wall. Four weeks post injection, the caecum and liver were harvested for further analysis.

Forced liver metastasis induction

Forced liver metastasis was induced by injecting cancer cells intrasplenically. Under anesthesia, the spleen was exposed and subsequently, 3.5×10^5 MC38 cancer cells dissolved in 100 µl PBS were intrasplenically injected using a 27-G needle, followed by a partial splenectomy. For MTOs, 3.5-5 x 10^5 cells dissolved in 100 µl HBSS were injected into each mouse. After 3 weeks, the mice were euthanized and the livers were harvested for further analysis. For anti-PD-L1 antibody treatment, 250 µg per mouse was injected intraperitoneally every 3 days. Anti-PD-L1 antibody administration was started 1 day post liver metastasis induction. For Foxp3+ Treg depletion, *DEREG* mice received 600 ng diphtheria toxin intraperitoneally, starting 1 day before liver metastasis induction, followed by weekly injections of 200 ng diphtheria toxin.

Immune cell isolation

Murine livers were harvested after PBS perfusion and gallbladder removal. Human samples were obtained from patients with CRC and resectable liver metastases at the Surgical Department of the University Medical Center Hamburg-Eppendorf. Murine and human tissues were cut into small pieces and digested in HBSS (with Ca^{2+} and Mg^{2+}) containing 10 U/ml DNase and 1 mg/ml collagenase, in a shaking incubator at 37 °C for 25 minutes. After digestion, the livers were smashed and washed using PBS (1% FBS) through a cell strainer to a single cell resolution, and the pellet was collected after centrifugation at 400 g for 8 minutes. Immune cells were then enriched from the pellet by Percoll gradient centrifugation (GE Healthcare, Chicago, IL). Human samples were obtained under the approval codes PV-3578 and PV-3548, which were approved by the local ethical committee "Ethik-Kommission der Ärztekammer Hamburg". Written informed consent was received from all participants prior to inclusion in this study.

Flow cytometry and fluorescent activated cell sorting

Hepatic immune cells or liver sinusoid endothelial cells (LSECs) were isolated as mentioned above. A monoclonal antibody (clone 2.4G2) was used to block the Fc-γ receptors. Then, the cells were washed and stained with fluorochrome-conjugated antibodies (Table S2). The BD LSRFortessa (BD Biosciences, San Jose, CA) was used for flow cytometry and FACSAria IIIu (BD Biosciences, San Jose, CA) was used for cell sorting. Data analysis was performed using FlowJo v.6.1 (TreeStar, Ashland, OR).

qPCR

Total RNA from cells or tissue was extracted with the TRIzol reagent (Invitrogen) and reverse transcribed with the High Capacity cDNA Reverse Transcription Kit according to the manufacturer's protocols (Life Technologies, Darmstadt, Germany). Real-time PCR was performed with the StepOne Plus (Life Technologies) using TaqMan probes, including *Il10* (Mm00439614_m1), *Il10ra* (Mm00434151_m1), *Il10rb* (Mm00434157_m1), *Hprt* (Mm03024075_m1), and *Granzyme B* (Mm00442837_m1). The level of gene expression was normalized to that of *Hprt*.

Statistical analysis

All data were analyzed using the GraphPad Prism statistical software (GraphPad software, San Diego, CA, USA). Mouse data are presented as mean ± SEM. The mRNA analysis is shown using a base 10 logarithm. Comparison of means was performed using the Mann-Whitney *U* test for paired group comparisons or the one-way ANOVA (Bonferroni) for multiple group comparisons. *P* values below 0.05 were considered significant.

Results

Impaired IL-10 signaling protects mice against CRC-derived liver metastasis

We first aimed to test the role of IL-10 in liver metastasis. To this end, LLC cancer cells were injected orthotopically into the cecum. Although the primary tumor weight was comparable in *Il10*-deficient and wild-type (WT) control mice (Fig. 1A,B), *Il10*-deficient mice developed less liver metastases compared to WT controls (Fig. 1C,D). We then confirmed this finding using murine colorectal liver metastasis (CRLM)-derived organoids, namely MTO129 (Fig. 1E,F), and MC38 cells (Fig. 1G,H). We observed reduced liver metastasis formation in *Il10*-deficient mice compared to WT littermates in both models. Next, to specifically investigate the role of IL-10 in CRLM development, we used an IL-10 receptor alpha (IL-10Ra) antibody, which was administered 1 day before metastasis induction, followed by injections every 3 days after induction. Indeed, IL-10Ra blockade during liver metastasis formation significantly decreased liver metastases (Fig. 1I,J). Finally, to test the impact of IL-10 on the primary tumor, we injected MC38 colon cancer cells intracecally and overall survival (humane endpoint) was assessed as a primary endpoint (Fig. S1A,B). In line with previous publications,[10] *Il10*-deficient mice had a lower survival rate and increased primary tumor growth compared to WT controls (Fig. S1A-C), a finding indicating a protective function of IL-10 in primary tumor development.

Taken together, these results demonstrated a pathogenic role of IL-10 signaling during liver metastasis formation.

The pathogenic role of IL-10 in liver metastasis formation is independent of colitis severity and the microbiome

Il10-deficient mice are known to be highly susceptible to spontaneous colitis manifestation.[6] Consequently, we next studied the impact of colitis development on liver metastasis. $Il10^{-/-}$ mice exhibited reduced liver metastases compared to littermate controls (Fig. S2A,B). Interestingly, these mice did not develop colitis during metastasis formation (Fig. S2C). We therefore induced colitis in $Il10^{-/-}$ mice and littermate controls using a colitogenic microbiome (Fig. S2D-F).[21] However, despite higher colitis severity observed in $Il10^{-/-}$ mice compared to littermate controls, the former were still protected from liver metastasis (Fig. S2G,H).

Taken together, *Il10*-deficient mice are protected from CRLM independently of colitis development.

Foxp3+Tregs are the major source of IL-10 in liver metastasis formation

Next, we aimed to identify the cellular source of IL-10 during liver metastasis formation. IL-10 is known to be widely expressed in various tissues and cells.[6] To define the cellular source of IL-10, a $Il10^{GFP}$;$Foxp3^{RFP}$ reporter mouse was used.[22] Increased IL-10 expression in hepatic immune cells, especially in CD4+ T cells, upon liver metastasis induction was observed (Fig. 2A-D). Of note, this upregulation was not seen in CD3-cells or CD8+ T cells. More specifically, an upregulation of IL-10 was found in Foxp3+Tregs, but not in Foxp3-IL-10+ cells (Fig. 2E-G). Immune cells, especially Foxp3+Tregs were also the major source of IL-10 in murine livers at steady state (Fig. S3A). Foxp3+Tregs further expanded along with liver metastasis formation (Fig. S3B,C), with a dynamically increased number that was IL-10+ (Fig. S3D,E). Indeed, Foxp3+Tregs contributed mostly to IL-10 production in established liver metastasis (Fig. 2H). Moreover, Foxp3+Treg depletion reduced liver metastatic load (Fig. S3F). Interestingly, the composition of IL-10-producing cells in primary CRC differed from that in liver metastases. Using the cecum cancer model, we found that the frequency of IL-10+ cells was mainly increased in CD3-cells, but not T cells (Fig. S4). Indeed, human samples from CRC and CRLM present distinct immune cell composition and therefore might account for different phenotypes regarding the different roles of IL-10 in primary CRC and CRLM (Fig. S5). Thus, our data indicated that the main IL-10-producing cells in primary CRC were non-T cells, as opposed to Foxp3+Tregs in liver metastases. To test the functional relevance of this finding, mice with a Foxp3+Treg-specific IL-10 deletion underwent liver metastasis induction via intrasplenic MC38 cell injection (Fig. 3A). Interestingly, mice bearing a Foxp3+Treg-specific IL-10 deletion were protected against liver metastasis compared to littermate controls (Fig. 3B). As a control, we also used mice with a myeloid cell-specific IL-10 deletion (LysmCre). Importantly, the liver metastatic burden did not differ between these groups (Fig. 3C).

Collectively, our results suggested that Foxp3+Tregs are the major functionally relevant source of IL-10 in liver metastasis.

IL-10 signaling in Foxp3+Tregs and myeloid cells promotes CRLM development

To further identify potential target cells of IL-10 during liver metastasis formation, IL-10Ra expression was analyzed in

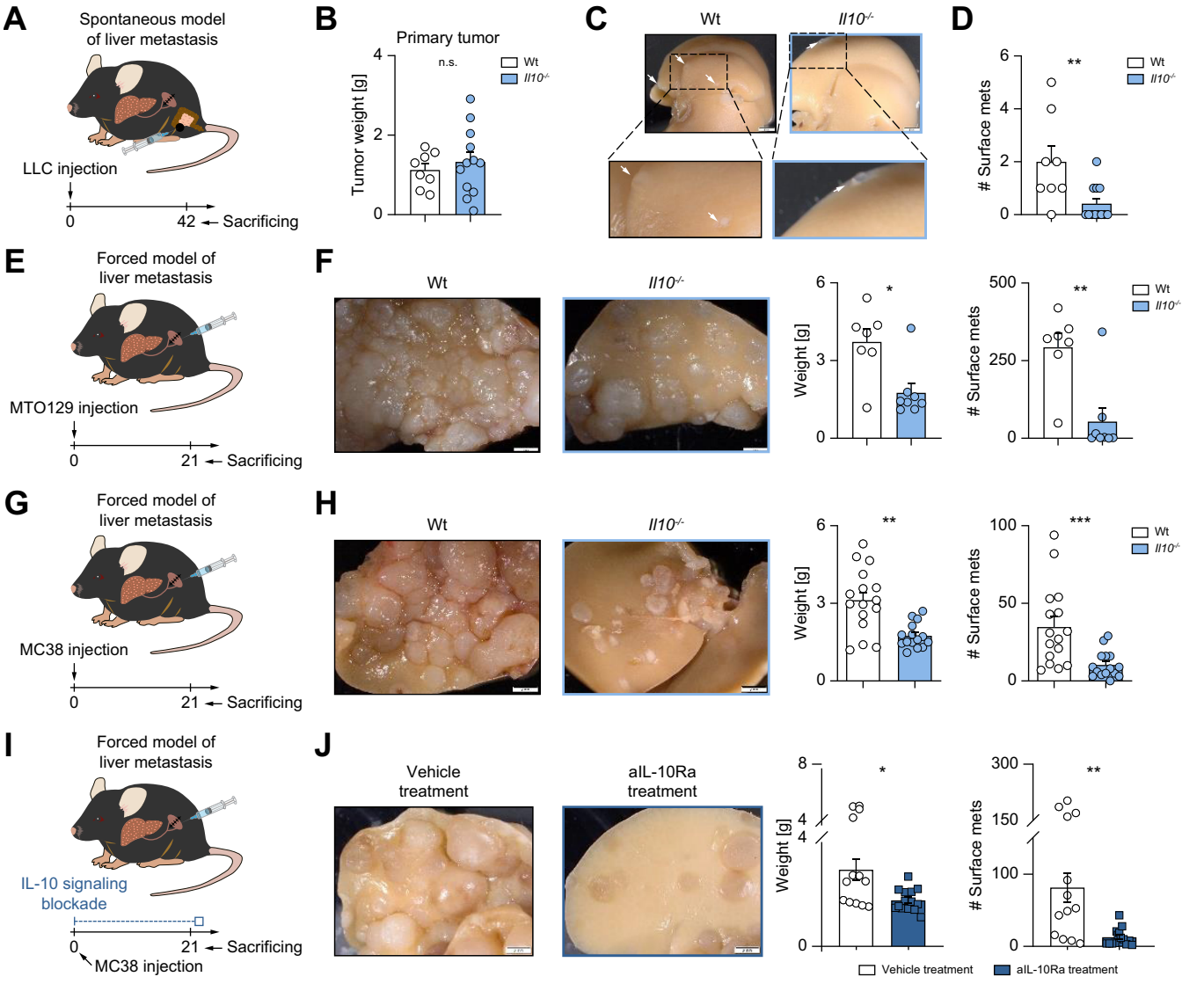

Fig. 1. Impaired IL-10 signaling protects mice against colorectal cancer-derived liver metastasis. (A) Schematic overview of intracecal LLC cancer cell injection for spontaneous liver metastasis induction. (B) Primary tumor weight in the cecum. (C) Representative pictures and (D) number of liver metastases in WT and *Il10*-/- mice (n ≥8 mice per group). (E) Schematic overview of MTO129 intrasplenic injection for forced liver metastasis induction. (F) Representative pictures of liver metastasis, metastatic load, including liver weight and number of macroscopic liver metastases in WT and *Il10*-/- mice (n ≥ 7 mice per group). (G) Schematic overview of intrasplenic MC38 cancer cell injection. (H) Representative pictures of liver metastasis, metastatic load in WT and *Il10*-/- mice (n ≥12 mice per group). (I) Schematic overview of WT mice receiving aIL-10Ra or isotype treatment during intrasplenic MC38 cell injection. (J) Representative pictures and analysis of liver weight and number of liver metastases (n ≥12 mice per group). Scale bar: 2 mm. Data are presented as mean ± SEM. Non-significant (n.s.): p >0.05; **p <0.01; ***p <0.001 calculated by Mann-Whitney *U* test. aIL-10Ra, IL-10 receptor alpha antibody; LLC, Lewis lung carcinoma; MC38, murine colon cancer cells; MTO, mouse tumor organoid; WT, wild-type. (This figure appears in color on the web.)

immune cells, cancer cells, hepatocytes and LSECs using qPCR and flow cytometry. Interestingly, innate cells and Foxp3+Tregs expressed the highest IL-10Ra levels among different immune cell subsets at steady state (Fig. 4A,B). Furthermore, they maintained high IL-10Ra expression in established liver metastasis (Fig. 4C,D). MC38 and LLC cancer cells showed no IL-10Ra expression (Fig. S6A,B). In liver cells, LSECs showed IL-10Ra expression, while the rest of the cells including hepatocytes showed only low or no IL-10Ra expression (Fig. S6C,D). We further examined STAT3 activation in these cells upon IL-10 stimulation *in vitro*. MC38 and LLC cancer cells did not respond to IL-10 (Fig. S6E), while LSECs (Fig. S6F,G) and immune cells (Fig. S6F) exhibited higher STAT3 phosphorylation after IL-10 stimulation *in vitro.* We have previously demonstrated that IL-22-mediated interactions between LSECs and immune cells promoted liver metastasis via enhancing cancer cell extravasation.[20] On this basis, we tested the role of IL-10 signaling in cancer cell extravasation using an intrasplenic injection of MC38-GFP cells in $Il10^{+/+}$ and $Il10^{-/-}$ mice (Fig. S6H). We found that extravasated cancer cells in the liver were comparable between these two groups 1 day post injection (Fig. S6I,J). Likewise, IL-10Ra deletion in LSECs did not significantly reduce liver metastases *in vivo* (Fig. S6K,L). We further analyzed different subsets of immune cells in response to IL-10 *in vitro*. We found that STAT3 signaling was activated in innate cells and Foxp3+Tregs, rather

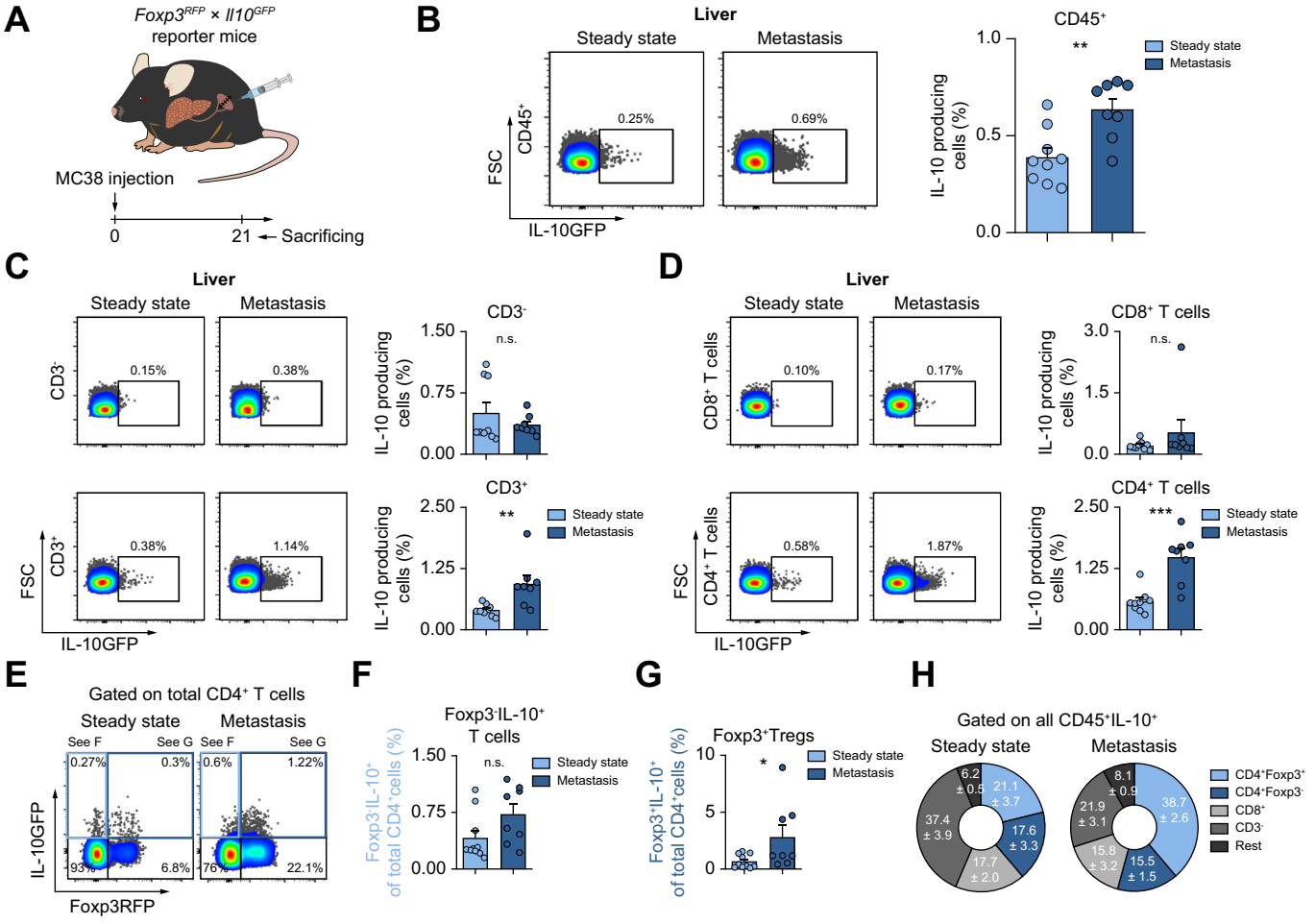

Fig. 2. Foxp3+Tregs are the major IL-10-producing cells during liver metastasis formation. (A) Schematic overview of intrasplenic MC38 cancer cell injection for forced liver metastasis induction in *Foxp3*^{RFP};*Il10*^{GFP} mice (n ≥8 mice per group). Frequency of IL-10+ cells in the fraction of (B) CD45+ cells, (C) CD3-and T cells, and in (D) CD8+ T cells and CD4+ T cells. (E) IL-10 expression in (F) Foxp3-IL-10+ cells and (G) Foxp3+Tregs. (H) General distribution of all IL-10-producing CD45+ cells in healthy liver and liver with metastasis. Data are presented as mean ± SEM. Non-significant (n.s.): p >0.05; *p ≤0.05; **p <0.01; ***p <0.001, as calculated by Mann-Whitney *U* test. MC38, murine colon cancer cells; Tregs, regulatory T cells. (This figure appears in color on the web.)

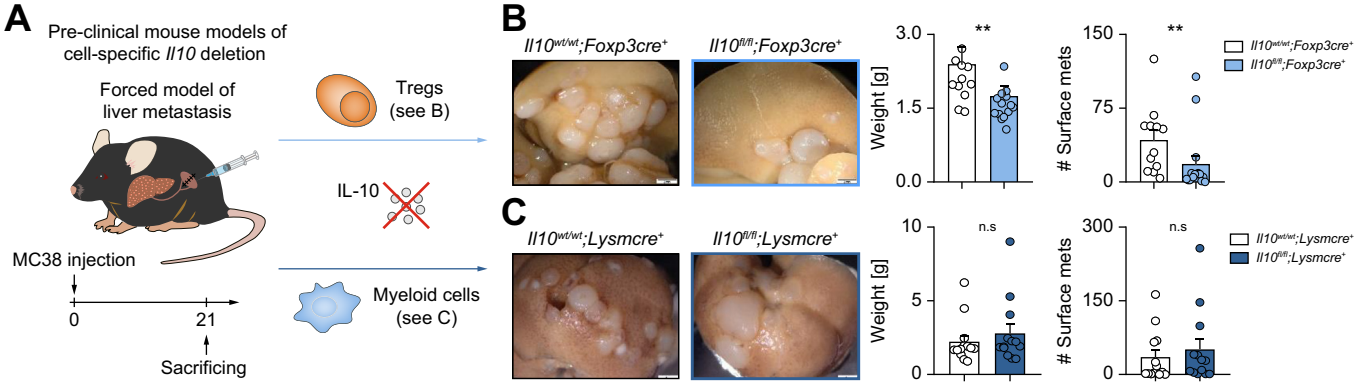

Fig. 3. Foxp3+Treg-derived IL-10 facilitates liver metastasis formation. (A) MC38 cells were intrasplenically injected into mice with cell-specific *Il10* deletion in Foxp3+Tregs and myeloid cells and their littermate controls (n ≥10 mice per group). Livers were harvested 21 days post injection. (B, C) Representative images, liver weight and number of liver metastases in mice with (B) Treg-specific or (C) myeloid cell-specific *Il10* deletion and their littermates. Scale bar: 2 mm. Data are presented as mean ± SEM. Non-significant (n.s.): p >0.05; **p <0.01, as calculated by Mann-Whitney *U* test. MC38, murine colon cancer cells; Tregs, regulatory T cells. (This figure appears in color on the web.)

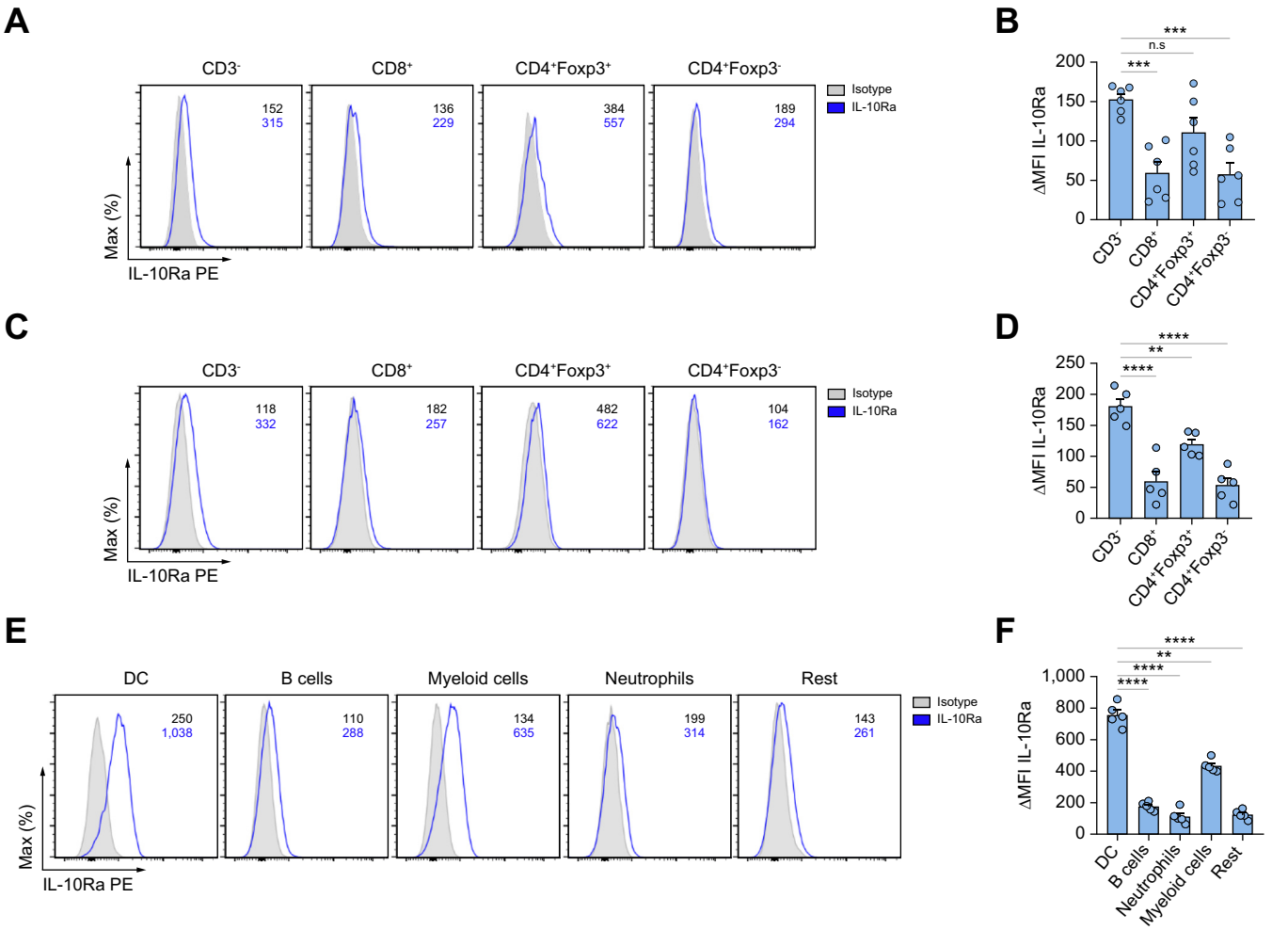

Fig. 4. Dendritic cells, myeloid cells and Foxp3+Tregs can respond to IL-10. (A–D) Representative FACS plot and ΔMFI quantification of IL-10Ra expression in immune cells isolated from (A, B) a healthy liver or (C, D) liver metastasis 21 days post intrasplenic cancer cell injection (n ≥5 mice per group). (E) Representative FACS plot and (F) ΔMFI quantification of IL-10Ra expression from different innate subsets (CD3-) in liver metastasis. Data are presented as mean ± SEM. Non-significant (n.s.): p >0.05; ***p <0.001, as calculated by Mann-Whitney U test or one-way ANOVA (Bonferroni) with Bonferroni *post hoc* tests. IL-10Ra, IL-10 receptor alpha; MFI, mean fluorescence intensity; Tregs, regulatory T cells. (This figure appears in color on the web.)

than CD8+ T cells and Foxp3-IL-10+ cells, upon IL-10 stimulation *in vitro* (Fig. S6M,N). In terms of non-T cells, myeloid cells, and especially dendritic cells (DCs), exhibited increased IL-10Ra expression compared to neutrophils, B cells, and other examined immune cell populations (Fig. 4E,F). Hence, myeloid cells and Foxp3+Tregs were identified as the main target cells of IL-10 during liver metastasis formation.

To further understand the outcome of IL-10 signaling on immune cells in the context of liver metastasis, we used cell-specific IL-10Ra-deficient mouse models (Fig. 5A). We injected MC38 cancer cells intrasplenically to establish liver metastasis in these mouse models and then compared their liver metastatic burden. Interestingly, IL-10 ablation in both Foxp3+Tregs (Fig. 5B) and myeloid cells (Fig. 5C) protected mice against liver metastasis. However, this protection was absent in mice with IL-10Ra deletion in DCs (Fig. 5D), suggesting a dispensable role of IL-10R signaling in DCs during liver metastasis formation. Additionally, IL-10Ra deletion in Foxp3+Tregs did not alter the frequency (Fig. S6O) of Foxp3+Tregs but decreased their *Il10* production upon IL-10 stimulation (Fig. S6P). Of note, IL-10 signaling ablation in IL-17-producing cells did not affect liver metastasis formation (Fig. 5E).

Taken together, IL-10 signaling in Foxp3+Tregs promotes their production of IL-10, which then acts on myeloid cells, thereby promoting CRLM.

IL-10 induces PD-L1 upregulation in monocytes, thereby attenuating CD8+ T-cell mediated immune surveillance

Finally, we aimed to decipher the underlying mechanism. Bulk sequencing of myeloid cells indicated that one of the inhibitory checkpoint ligands, PD-L1, was reduced in *Il10ra*$^{fl/fl}$;*Lysm*$^{cre+}$ mice compared to littermate controls (Fig. S7A). Thus, we hypothesized that IL-10 may regulate the PD-L1/PD-1 axis between myeloid cells and cytotoxic T cells, thereby affecting antitumor immunity. To test this hypothesis, PD-L1 expression was assessed in hepatic myeloid cells isolated from myeloid cell-specific IL-10Ra-deficient mice and littermate controls after liver metastasis induction (Fig. 6A). PD-L1 expression in myeloid cells was downregulated in the absence of IL-10Ra in myeloid

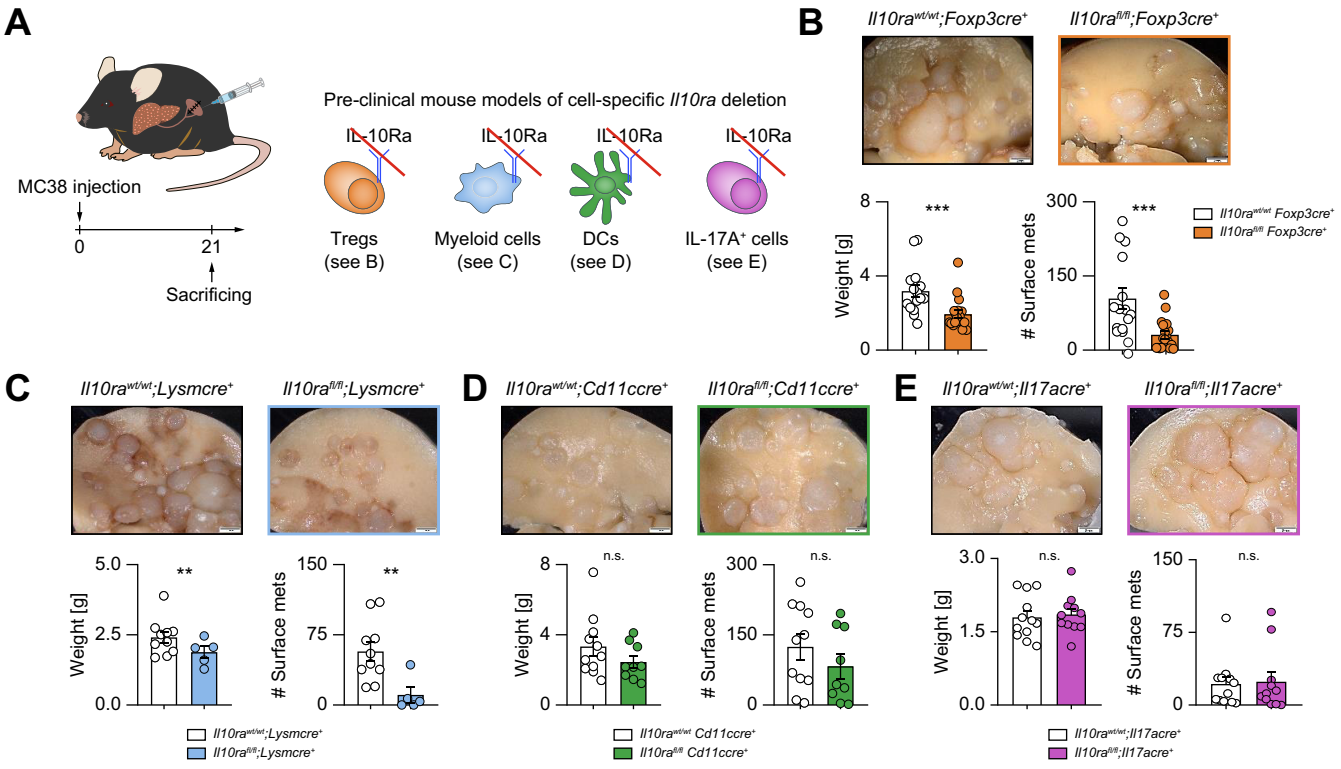

Fig. 5. IL-10 signaling in Foxp3+Tregs and myeloid cells promotes colorectal cancer-derived liver metastasis. (A) Schematic overview of intrasplenic MC38 cancer cell injection in mice with distinct cell-specific *Il10ra* deletion (n ≥5 mice per group). Representative images, liver weight and number of liver metastases in mice with (B) Treg-, (C) myeloid-, (D) DC-, or (E) Th17-specific *Il10ra* deletion. Scale bar: 2 mm. Data are presented as mean ± SEM. Non-significant (n.s.): $p > 0.05$; *$p \leq 0.05$; **$p < 0.01$; ***$p < 0.001$, as calculated by Mann-Whitney *U* test. DC, dendritic cell; Il10ra, IL-10 receptor alpha; MC38, murine colon cancer cells; Th17, T helper 17 cells; Tregs, regulatory T cells. (This figure appears in color on the web.)

cells (Fig. 6B). Additionally, this IL-10 signaling-dependent PD-L1 regulation was further validated in myeloid cells, specifically monocytes (Fig. 6C and Fig. S7B,C). Furthermore, PD-L1 deletion protected mice against liver metastasis formation (Fig. S7D). Next, we aimed to test whether this IL-10 signaling in myeloid cells indeed affects antitumor immunity of CD8+ T cells and cancer cell killing. We first induced liver metastasis using an intrasplenic injection of MC38 cells in myeloid cell-specific IL-10Ra-deficient mice and littermate controls. From these mice we then isolated CD8+ T cells from liver metastases, and cocultured them with MC38 cancer cells. Subsequently, antitumor factor granzyme B within CD8+ T cells was assessed, as well as cancer cell apoptosis via Annexin V and PI staining (Fig. 6D,E). Higher CD8+ T cell-produced granzyme B levels and increased cancer cell apoptosis were observed in *Il10ra*$^{fl/fl}$;*Lysm*$^{cre+}$ mice compared to their littermate controls (Fig. 6D,E). To confirm if the effect on CD8+ T cells and cancer cells was dependent on PD-L1, we characterized CD8+ T cells in *Pdl1*$^{+/+}$ and *Pdl1*$^{-/-}$ mice after injecting MC38 cells intrasplenically. Increased tumor-infiltrating CD8+ T cells with similar granzyme B mRNA production was detected in *Pdl1*$^{-/-}$ mice compared to littermate control (*Pdl1*$^{+/+}$) mice (Fig. S7E,F). After coculture with MC38 cells, tumor-infiltrating CD8+ cells in *Pdl1*$^{-/-}$ mice expressed much higher amounts of granzyme B compared to *Pdl1*$^{+/+}$ mice (Fig. S7G). To confirm that the pro-metastatic role of myeloid cell-dependent IL-10 signaling was mediated by PD-L1, PD-L1 blockade treatment was administrated to *Il10ra*$^{fl/fl}$;*Lysm*$^{cre+}$ mice and their littermate controls upon liver metastasis induction. Deletion of IL-10Ra in myeloid cells reduced metastasis formation in the absence of a PD-L1 antibody. However, in the presence of a PD-L1 antibody, the deletion of IL-10Ra did not impact metastasis formation (Fig. 6F). These data indicate that the effect of IL-10 signaling in myeloid cells is, at least in part, dependent on PD-L1 expression.

Overall, we demonstrated that IL-10 induces PD-L1 expression in monocytes, thereby attenuating CD8+ T-cell infiltration and antitumor immunity, ultimately facilitating liver metastasis formation.

Discussion

The liver is one of the most susceptible sites to metastasis from various malignancies, for example, CRC, breast cancer and melanoma. Overall, CRC remains the most common primary tumor leading to liver metastasis.[23] Most patients with CRC develop CRLM during the course of disease, even after curative resection of the primary tumor. Currently, standard treatment options against liver metastasis consist of surgical resection and chemotherapy. However, even if detected at an early stage, a considerable number of liver metastases cannot be surgically removed.[24] Thus, controlling liver metastasis remains challenging and metastasis is still the major contributor to CRC-related death.[25]

Notably, immunotherapy has, in certain instances, led to remarkable responses in inoperable malignancies, such as melanoma and small cell lung cancer.[26] Specifically, immune checkpoint inhibitors have been found to restore antitumor T cells and suppress tumor development. Anti-PD-1 and anti-PD-

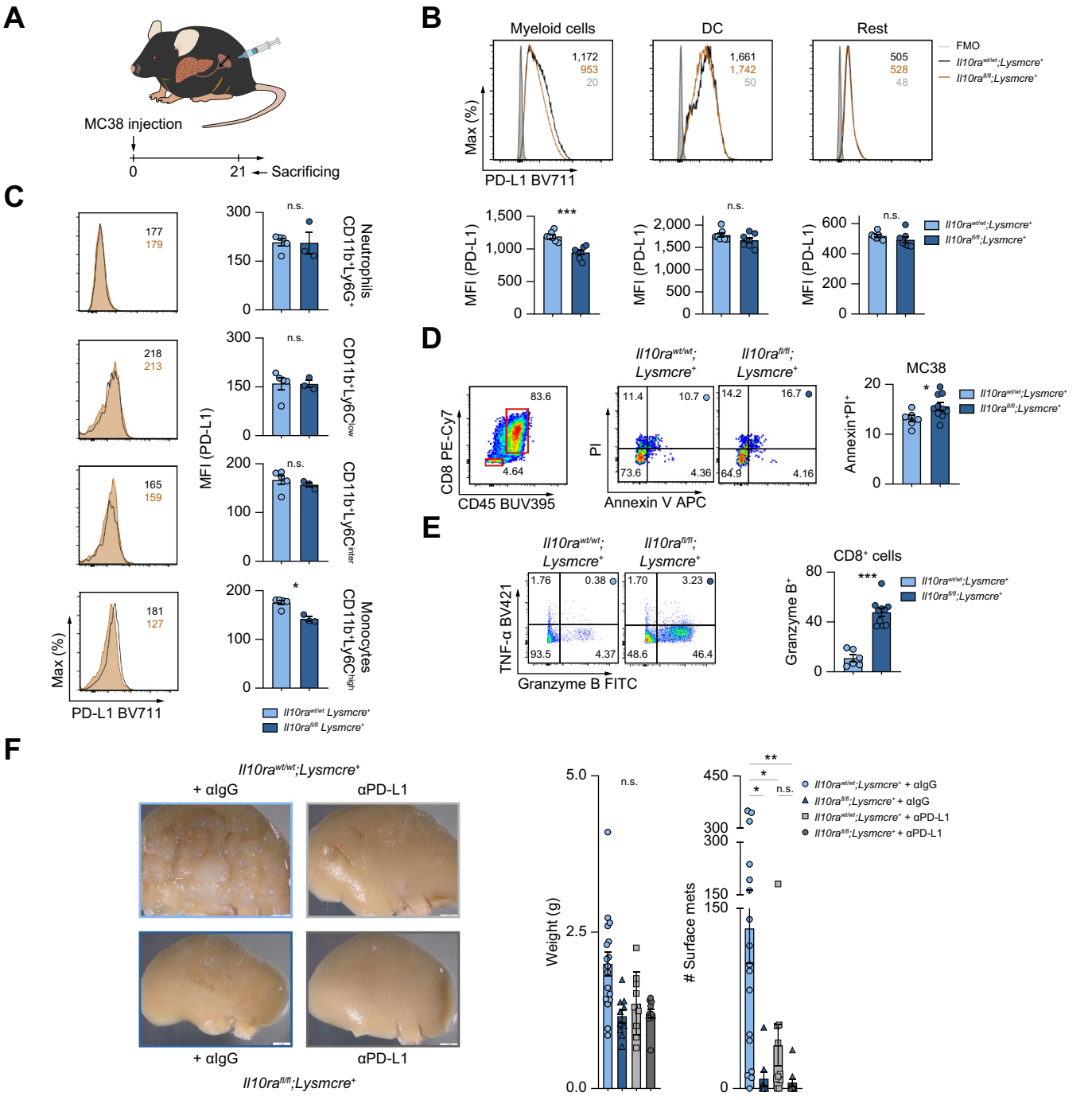

Fig. 6. IL-10-mediated PD-L1 upregulation in monocytes attenuates CD8+ T-cell infiltration and antitumor immunity. (A) Schematic overview of intrasplenic MC38 cancer cell injection in mice with myeloid-specific *Il10ra* deletion and their littermate controls (n ≥3 mice per group). (B, C) Representative FACS plot and MFI quantification of PD-L1 expression in (B) myeloid cells, DCs and remaining innate cells, as well as in (C) indicated subpopulations within myeloid cells. 14 days post injection, (D) apoptosis of MC38 cells and (E) antitumor immunity (TNF-α and granzyme B) of CD8+ T cells were analyzed using flow cytometry. (F) Mice with myeloid-specific *Il10ra* deletion and their littermate controls, receiving anti-IgG or anti-PD-L1 (250 μg/mouse) were injected intrasplenically with MC38 cancer cells (n ≥9 mice per group). Number of liver metastases was quantified 21 days post liver metastasis induction. Scale bar: 2 mm. Data are presented as mean ± SEM. Non-significant (n.s.): $p > 0.05$; *$p \leq 0.05$; **$p < 0.01$; ***$p < 0.001$, as calculated by one-way ANOVA (Bonferroni) with Bonferroni *post hoc* tests. . IL-10Ra, IL-10 receptor alpha; MC38, murine colon cancer cells; MFI, mean fluorescence intensity; (a)PD-L1, programmed cell death ligand 1 (antibody); TNF-α, tumor necrosis factor-alpha. (This figure appears in color on the web.)

L1 antibodies are the most studied and attractive immune checkpoint inhibitors that have shown therapeutic potential against primary cancers and metastases.[25,26] However, the presence of liver metastasis has been reported to reduce cytotoxic CD8+ T-cell numbers and restrain the effect of immunotherapy.[4] Unfortunately, the underlying mechanism is unclear.

Interestingly, a recent *in vitro* study found that IL-10 blockade in organotypic slides from patients with metastatic CRC increased activated CD8+ frequency and enhanced the

activation and cytotoxicity of CAR-T cells, leading to higher cancer cell apoptosis.[27] These data suggest that IL-10 signaling may play an important role in CRLM. However, the *in vivo* relevancy of IL-10, the source and potential mechanism of action remain unclear. Furthermore, IL-10 has been implicated in the pathogenesis of multiple diseases, such as chronic infectious diseases and cancer.[6,28,29] A recent study reported upregulated IL-10 levels in murine liver metastasis compared to healthy controls.[30] Interestingly, lower serum IL-10 levels correlated with higher occurrence and poorer prognosis of CRC.[31] Furthermore, a protective role of IL-10 in lung metastasis was reported.[10] However, the role of IL-10 in liver metastasis *in vivo* was unclear. Therefore, in this study, we aimed to decipher the role of IL-10 in liver metastasis and to determine how its modulation could be used to enhance the efficacy of immunotherapy *in vivo*.

In line with previous findings,[28] we observed that IL-10 was upregulated in metastatic sites compared to healthy liver in mouse. The role of IL-10 in various cancer types seems to be controversial.[32] Herein, we used spontaneous and forced mouse models of liver metastasis. We found that IL-10 inhibited primary CRC, while it promoted CRLM. Interestingly, the cellular source of IL-10 was different between the primary CRC and CRLM: we identified Foxp3+Tregs as the main cellular source of IL-10 during liver metastasis formation, while innate cells were the main cellular source of IL-10 in primary CRC in our model. This different cellular source may explain the different roles of IL-10. This is in line with recent studies demonstrating different immune cell compositions in human CRC and CRLM.[33,34] To provide more evidence, we also characterized the immune composition in human samples from CRC and CRLM. In CRC, B-cell frequency decreased in tumor tissue compared to peritumor tissue. In contrast, in CRLM, reduced innate cells and increased T cells were present in metastases. Within T cells, CD4+ and CD8+ cell frequency was not altered in CRC, while a higher CD4+ T-cell and lower CD8+ T-cell frequency was observed in CRLM compared to peri-metastatic liver. However, further studies will be important to address this point. Next, we performed flow cytometry to measure IL-10Ra expression among immune cells, cancer cells, hepatocytes and LSECs. We found that T cells do express lower amounts of IL-10Ra and thus have a lower STAT3 activation upon IL-10 treatment compared to innate cells. This is in line with our previous publications.[35] As the IL-10Ra expression was low in T cells, we conducted functional *in vitro* and *in vivo* experiments in order to show that the expression is still biologically relevant. By using cell-specific IL-10Ra-deficient mouse models, we found that IL-10Ra depletion in myeloid cells and Foxp3+Tregs resulted in significantly less liver metastasis. Consistent with previous studies analyzing the role of IL-10Ra on Foxp3+Tregs during colitis,[28] we showed that IL-10 signaling in Foxp3+Tregs was important to boost IL-10 production. Furthermore, impaired IL-10 signaling in Foxp3+Tregs did not affect the frequency of Foxp3+Tregs. Thus, we suggest that IL-10Ra depletion on Foxp3+Tregs influences IL-10 production, which subsequently impairs IL-10 signaling in myeloid cells and thereby affects liver metastatic burden.

Next, we aimed to identify the mechanism underlying the pathogenic myeloid cell-mediated role of IL-10 signaling in liver metastasis formation. It was reported that Tregs, together with CD11b+ monocytes, are associated with immune suppression in liver metastasis.[36] In addition, a combination of Treg depletion and an anti-PD-1 therapy, instead of an anti-PD-1 monotherapy, was shown to improve antitumor immunity.[36] However, the molecular mechanism underlying this immune suppression is not clear. Surprisingly, our data shows a downregulation of PD-L1 in myeloid cells upon IL-10Ra deletion during liver metastasis formation. Specifically, monocytes are the most affected myeloid cell population. Moreover, it has previously been reported that anti-PD-L1 blockade on monocytes can lead to a greater T-cell expansion in the context of asymptomatic multiple myeloma.[37] Previous studies have demonstrated that PD-L1 depletion in DCs increases CD8+ T-cell responses and reduces tumor growth.[38] However, in CRC-derived liver metastasis, IL-10-mediated PD-L1 regulation was not found in DCs but in monocytes. Additionally, IL-10Ra deficiency in DCs did not alter liver metastatic burden in our mouse models.

To understand the role of PD-L1 in CRLM, we first used PD-L1-deficient mice and showed that PD-L1 deficiency resulted in significantly lower liver metastatic burden, a higher frequency of tumor-infiltrating CD8+ T cells as well as a higher total amount of granzyme B expression. Consistent with this, tumor-infiltrating CD8+ T cells from myeloid cell-specific IL-10Ra-deficient mice aggravated cancer cell apoptosis, while also exhibiting a higher granzyme B expression. Importantly, using anti-PD-L1 in myeloid cell-specific *Il10ra*-deficient mice, we observed that the effect of IL-10 signaling in myeloid cells on liver metastasis formation was at least in part dependent on PD-L1. However, our data do not exclude an additional role of other factors, such as IFN-γ. Further studies are required to test the role of these factors. Taken together, we demonstrated that IL-10 signaling mediated the regulation of PD-L1 on monocytes, and thus, affected cancer cell apoptosis through modulation of CD8+ T cell-mediated antitumor immunity. This suggests a potential mechanism underlying resistance to immunotherapy in patients with liver metastasis and emphasizes the importance of controlling IL-10 levels in such patients.

There have been contrasting reports regarding PD-L1/PD-1 interactions between monocytes and T cells.[39–41] It was reported that monocyte-expressed PD-1 could affect T memory cell-mediated antitumor immunity.[41] Interestingly, we showed that monocyte-expressed PD-L1 could attenuate CD8+ T-cell infiltration, and thus antitumor immunity, specifically via granzyme B expression. Of note, the combination of anti-PD-L1 and IL-10Ra depletion in myeloid cells produced the best clinical outcome upon metastasis induction in mice. This provides a novel treatment option for combining anti-PD-L1 and anti-IL-10Ra in patients with CRLM, especially those who do not respond to immunotherapy.

In conclusion, our data provide evidence that Foxp3+Treg-produced IL-10 upregulates PD-L1 expression in monocytes, which in turn reduces CD8+ T-cell infiltration and related antitumor immunity, thereby promoting CRLM formation. These findings highlight the potential therapeutic benefit of a novel combined anti-IL-10Ra and anti-PD-L1 approach against CRLM.

Affiliations

[1]*Section of Molecular Immunology and Gastroenterology, I. Department of Medicine, University Medical Center Hamburg-Eppendorf, 20246, Hamburg, Germany;* [2]*Hamburg Center for Translational Immunology (HCTI), University Medical Center Hamburg-Eppendorf, 20246 Hamburg, Germany;* [3]*Division for Experimental Feto-Maternal Medicine, Department of Obstetrics and Fetal Medicine, University Medical Center of Hamburg-Eppendorf, Hamburg, Germany;* [4]*University Children's Hospital, University Medical Center of Hamburg-Eppendorf, Hamburg, Germany;* [5]*Department of General, Visceral and Thoracic Surgery, University Medical Center Hamburg-Eppendorf, Hamburg 20246, Germany;* [6]*Department of Medical Oncology, Erasmus MC Cancer Institute, University Medical Center Rotterdam, The Netherlands;* [7]*Institute for Research in Biomedicine (IRB Barcelona), The Barcelona Institute of Science and Technology (BIST), Barcelona, Spain;* [8]*Centro de Investigación Biomédica en Red de Cáncer (CIBERONC), Barcelona, Spain;* [9]*Institució Catalana de Recerca i Estudis Avançats (ICREA), Barcelona, Spain;* [10]*Mildred Scheel Cancer Career Center HaTriCS4, University Medical Center Hamburg-Eppendorf, 20246 Hamburg, Germany;* [11]*Research Department Cell and Gene Therapy, Department of Stem Cell Transplantation, University Medical Center Hamburg-Eppendorf, Hamburg 20246, Germany;* [12]*Protozoa Immunology, Bernard-Nocht-Institute for Tropical Medicine, 20359 Hamburg, Germany;* [13]*3rd Department of Surgery, National & Kapodistrian University of Athens, Greece;* [14]*Division of Surgery & Interventional Science, University College London (UCL), UK;* [15]*Department of Immunobiology, School of Medicine, Yale University, New Haven, CT 06520, USA;* [16]*Howard Hughes Medical Institute, Yale University School of Medicine, New Haven, CT 06520, USA*

Abbreviations

CAR-T, chimeric antigen receptor T; CRC, colorectal cancer; CRLM, colorectal liver metastasis; DCs, dendritic cells; IL-10Ra, IL-10 receptor alpha; LLC, Lewis lung carcinoma; LSECs, liver sinusoidal endothelial cells; MC38, murine colon cancer cells; MTO, mouse tumor organoid; PD-1, programmed death 1; PD-L1, programmed death ligand 1; Tregs, regulatory T cells; WT, wild-type.

Financial support

This work was supported in part by the Deutsche Forschungsgemeinschaft (DFG) (SFB841 to S.H.), the European Research Council (CoG 865466 to S.H.), Else Kröner Memorial Stipendium (A.D.G. and J.K), Erich und Gertrud Roggenbuck-Stiftung (A.D.G.), Hamburger Krebsgesellschaft Stiftung (A.D.G.) and the Jung Foundation for Science and Research (A.D.G.), Werner Otto Stiftung (J.K.), China Scholarship Council (T.Z.), Mildred Scheel Cancer Career Center Hamburg HaTriCS4 (funded by Deutsche Krebshilfe; J.K.). P.M.L. receives speaker fees from MSD. N.G. receives research grants from F. Hoffmann-La Roche and DZIF. S.H. has an endowed Heisenberg-Professorship awarded by the Deutsche Forschungsgemeinschaft.

Conflict of interest

N.G. reports financial support from F. Hoffmann-La Roche. This is outside the submitted work. Other authors declare no conflict of interest.

Please refer to the accompanying ICMJE disclosure forms for further details.

Authors' contributions

A.M.S., T.Z., and A.D.G. conceived, designed, and carried out most experiments, analyzed data, and wrote the manuscript; T.B., D.E.Z., L.Z., J.L., J.K., M.N. carried out *in vivo* experiments and flow cytometry assays; A.F. performed organoids culture and preparation for injection. S.Z. performed qPCR. D.V.T., E.B. provided mouse organoids and provided technical consult. B.S. analyzed RNA sequencing data. K.R. and T.A. constructed expression vectors and performed transfection experiments; Y.X. and L.B. performed fluorescence-activated cell sorting; I.L. performed in vivo experiments; L.K., L.B., B.M., P.S., N.K., P.M.L, A.H., P.C.A., B.F., P.B., R.G., O.M., J.R.I, T.H. provided critical intellectual input; N.G. designed experiments, provided critical intellectual input, and edited the paper; A.D.G. and S.H. conceived the idea and supervised the study, designed experiments, and wrote the manuscript. All authors reviewed and concurred with the submitted manuscript.

Data availability statement

All data from this study are provided in the source data. Primary data from flow cytometry or qPCR are available upon reasonable request. The accession number for the bulk seq data is GSE247304.

Acknowledgements

The authors thank Cathleen Haueis, Sandra Wende, and Tom Blankenburg for technical assistance, the *in vivo* Optical Imaging Core Facility and the Cytometry und Cell Sorting Core Unit at the University Medical Center Hamburg-Eppendorf for their technical assistance. *Pdl1*$^{-/-}$ mice were kindly provided by Dr. Gisa Tiegs as part of an ongoing collaboration.

Supplementary data

Supplementary data to this article can be found online at https://doi.org/10.1016/j.jhep.2023.12.015.

References

Author names in bold designate shared co-first authorship

[1] Esposito M, Ganesan S, Kang Y. Emerging strategies for treating metastasis. Nat Cancer 2021;2:258–270.

[2] Bray F, Ferlay J, Soerjomataram I, et al. Global cancer statistics 2018: GLOBOCAN estimates of incidence and mortality worldwide for 36 cancers in 185 countries. CA: A Cancer J Clinicians 2018;68:394–424.

[3] Obenauf AC, Massagué J. Surviving at a distance: organ-specific metastasis. Trends Cancer 2015;1:76–91.

[4] **Yu J**, **Green MD**, Li S, et al. Liver metastasis restrains immunotherapy efficacy via macrophage-mediated T cell elimination. Nat Med 2021;27:152–164.

[5] **Wei XL**, **Luo X**, **Sheng H**, et al. PD-L1 expression in liver metastasis: its clinical significance and discordance with primary tumor in colorectal cancer. J Transl Med 2020;18:475.

[6] **Bedke T**, **Muscate F**, Soukou S, et al. IL-10-producing T cells and their dual functions. Semin Immunol 2019;44:101335.

[7] **Guo Y**, **Xie YQ**, Gao M, et al. Metabolic reprogramming of terminally exhausted CD8(+) T cells by IL-10 enhances anti-tumor immunity. Nat Immunol 2021;22:746–756.

[8] Mumm JB, Emmerich J, Zhang X, et al. IL-10 elicits IFNγ-dependent tumor immune surveillance. Cancer Cell 2011;20:781–796.

[9] **Qiao J**, **Liu Z**, **Dong C**, et al. Targeting tumors with IL-10 prevents dendritic cell-mediated CD8(+) T cell apoptosis. Cancer Cell 2019;35:901–915.e904.

[10] **Tanikawa T**, **Wilke CM**, Kryczek I, et al. Interleukin-10 ablation promotes tumor development, growth, and metastasis. Cancer Res 2012;72:420–429.

[11] Naing A, Wong DJ, Infante JR, et al. Pegilodecakin combined with pembrolizumab or nivolumab for patients with advanced solid tumours (IVY): a multicentre, multicohort, open-label, phase 1b trial. Lancet Oncol 2019;20:1544–1555.

[12] Spigel D, Jotte R, Nemunaitis J, et al. Randomized phase 2 studies of checkpoint inhibitors alone or in combination with pegilodecakin in patients with metastatic NSCLC (CYPRESS 1 and CYPRESS 2). J Thorac Oncol 2021;16:327–333.

[13] Oft M. Immune regulation and cytotoxic T cell activation of IL-10 agonists - preclinical and clinical experience. Semin Immunol 2019;44:101325.

[14] **Sullivan KM**, **Jiang X**, Guha P, et al. Blockade of interleukin 10 potentiates antitumour immune function in human colorectal cancer liver metastases. Gut 2023 Feb;72(2):325–337.

[15] Rubtsov YP, Rasmussen JP, Chi EY, et al. Regulatory T cell-derived interleukin-10 limits inflammation at environmental interfaces. Immunity 2008;28:546–558.

[16] **Yogev N**, **Bedke T**, **Kobayashi Y**, et al. CD4(+) T-cell-derived IL-10 promotes CNS inflammation in mice by sustaining effector T cell survival. Cell Rep 2022;38:110565.

[17] Giannou AD, Marazioti A, Spella M, et al. Mast cells mediate malignant pleural effusion formation. J Clin Invest 2015;125:2317–2334.

[18] Weber K, Bartsch U, Stocking C, et al. A multicolor panel of novel lentiviral "gene ontology" (LeGO) vectors for functional gene analysis. Mol Ther 2008;16:698–706.

[19] Tauriello DVF, Palomo-Ponce S, Stork D, et al. TGFbeta drives immune evasion in genetically reconstituted colon cancer metastasis. Nature 2018;554:538–543.

[20] **Giannou AD**, **Kempski J**, **Shiri AM**, et al. Tissue resident iNKT17 cells facilitate cancer cell extravasation in liver metastasis via interleukin-22. Immunity 2023;56:125–142 e112.

[21] **Palm NW**, **de Zoete MR**, Cullen TW, et al. Immunoglobulin A coating identifies colitogenic bacteria in inflammatory bowel disease. Cell 2014;158:1000–1010.
[22] **Kamanaka M**, **Kim ST**, Wan YY, et al. Expression of interleukin-10 in intestinal lymphocytes detected by an interleukin-10 reporter knockin tiger mouse. Immunity 2006;25:941–952.
[23] Tsilimigras DI, Brodt P, Clavien PA, et al. Liver metastases. Nat Rev Dis Primers 2021;7:27.
[24] Hu DD, Pan YX, Chen G. Colorectal cancer liver metastases: an update of treatment strategy and future perspectives. Surg Pract Sci 2021:7.
[25] **Zhou H**, **Liu Z**, Wang Y, et al. Colorectal liver metastasis: molecular mechanism and interventional therapy. Signal Transduct Target Ther 2022;7:70.
[26] **Edwards SC**, **Hoevenaar WHM**, Coffelt SB. Emerging immunotherapies for metastasis. Br J Cancer 2021;124:37–48.
[27] **Sullivan KM**, **Jiang X**, Guha P, et al. Blockade of interleukin 10 potentiates antitumour immune function in human colorectal cancer liver metastases. Gut 2023;72:325–337.
[28] **Rallis KS**, **Corrigan AE**, **Dadah H**, et al. IL-10 in cancer: an essential thermostatic regulator between homeostatic immunity and inflammation - a comprehensive review. Future Oncol 2022;18:3349–3365.
[29] Saraiva M, Vieira P, O'Garra A. Biology and therapeutic potential of interleukin-10. J Exp Med 2020:217.
[30] **Huang XM**, **Zhang NR**, **Lin XT**, et al. Antitumor immunity of low-dose cyclophosphamide: changes in T cells and cytokines TGF-beta and IL-10 in mice with colon-cancer liver metastasis. Gastroenterol Rep (Oxf) 2020;8:56–65.
[31] Abtahi S, Davani F, Mojtahedi Z, et al. Dual association of serum interleukin-10 levels with colorectal cancer. J Cancer Res Ther 2017;13:252–256.
[32] Mannino MH, Zhu Z, Xiao H, et al. The paradoxical role of IL-10 in immunity and cancer. Cancer Lett 2015;367:103–107.
[33] **Wu Y**, **Yang S**, **Ma J**, et al. Spatiotemporal immune landscape of colorectal cancer liver metastasis at single-cell level. Cancer Discov 2022;12:134–153.
[34] **Liu Y**, **Zhang Q**, Xing B, et al. Immune phenotypic linkage between colorectal cancer and liver metastasis. Cancer Cell 2022;40:424–437 e425.
[35] Kamanaka M, Huber S, Zenewicz LA, et al. Memory/effector (CD45RB(lo)) CD4 T cells are controlled directly by IL-10 and cause IL-22-dependent intestinal pathology. J Exp Med 2011;208:1027–1040.
[36] Lee JC, Mehdizadeh S, Smith J, et al. Regulatory T cell control of systemic immunity and immunotherapy response in liver metastasis. Sci Immunol 2020;5.
[37] Bar N, Costa F, Das R, et al. Differential effects of PD-L1 versus PD-1 blockade on myeloid inflammation in human cancer. JCI Insight 2020;5.
[38] Oh SA, Wu DC, Cheung J, et al. PD-L1 expression by dendritic cells is a key regulator of T-cell immunity in cancer. Nat Cancer 2020;1:681–691.
[39] Diskin B, Adam S, Cassini MF, et al. PD-L1 engagement on T cells promotes self-tolerance and suppression of neighbor-ing macrophages and effector T cells in cancer. Nat Immunol 2020;21:442–454.
[40] Strauss L, Mahmoud MAA, Weaver JD, et al. Targeted deletion of PD-1 in myeloid cells induces antitumor immunity. Sci Immunol 2020;5.
[41] Akbay EA, Koyama S, Liu Y, et al. Interleukin-17A promotes lung tumor progression through neutrophil attraction to tumor sites and mediating resistance to PD-1 blockade. J Thorac Oncol 2017;12:1268–1279.

Journal of Hepatology, Volume *80*

Supplemental information

IL-10 dampens antitumor immunity and promotes liver metastasis via PD-L1 induction

Ahmad Mustafa Shiri, Tao Zhang, Tanja Bedke, Dimitra E. Zazara, Lilan Zhao, Jöran Lücke, Morsal Sabihi, Antonella Fazio, Siwen Zhang, Daniele V.F. Tauriello, Eduard Batlle, Babett Steglich, Jan Kempski, Theodora Agalioti, Mikołaj Nawrocki, Yang Xu, Kristoffer Riecken, Imke Liebold, Leonie Brockmann, Leonie Konczalla, Lidia Bosurgi, Baris Mercanoglu, Philipp Seeger, Natalie Küsters, Panagis M. Lykoudis, Asmus Heumann, Petra C. Arck, Boris Fehse, Philipp Busch, Rainer Grotelüschen, Oliver Mann, Jakob R. Izbicki, Thilo Hackert, Richard A. Flavell, Nicola Gagliani, Anastasios D. Giannou, and Samuel Huber

IL-10 dampens antitumor immunity and promotes liver metastasis via PD-L1 induction

Ahmad Mustafa Shiri, Tao Zhang, Tanja Bedke, Dimitra E. Zazara, Lilan Zhao, Jöran Lücke, Morsal Sabihi, Antonella Fazio, Siwen Zhang, Daniele V.F. Tauriello, Eduard Batlle, Babett Steglich, Jan Kempski, Theodora Agalioti, Mikołaj Nawrocki, Yang Xu, Kristoffer Riecken, Imke Liebold, Leonie Brockmann, Leonie Konczalla, Lidia Bosurgi, Baris Mercanoglu, Philipp Seeger, Natalie Küsters, Panagis M. Lykoudis, Asmus Heumann, Petra C. Arck, Boris Fehse, Philipp Busch, Rainer Grotelüschen, Oliver Mann, Jakob R. Izbicki, Thilo Hackert, Richard A. Flavell, Nicola Gagliani, Anastasios D. Giannou, Samuel Huber

Table of contents

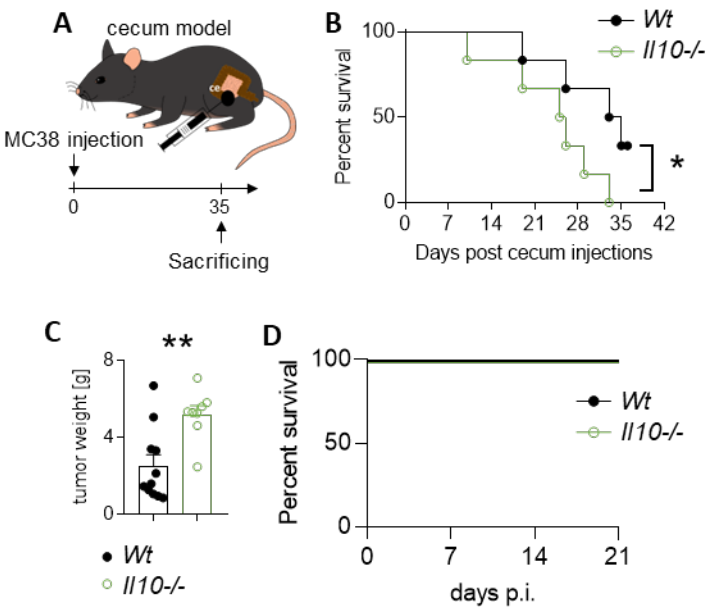

Fig. S1: *Il10*-deficiency in mouse promotes primary tumor growth

(**A**) Schematic overview of the intracaecal injection of MC38 cancer cells for spontaneous liver metastasis induction. (**B**) Overall survival and (**C**) Primary tumor weight in the caecum of *Wt* and *Il10-/-* mice (n ≥ 8 mice per group). (**D**) Overall survival of the mice after intrasplenic injection of MC38 cells. Data are presented as mean ± SEM. Non-significant (ns): $p > 0.05$; *: $p \leq 0.05$; **: $p < 0.01$, as calculated by Mantel-Cox test or Mann-Whitney *U* test. p.i.: post injection

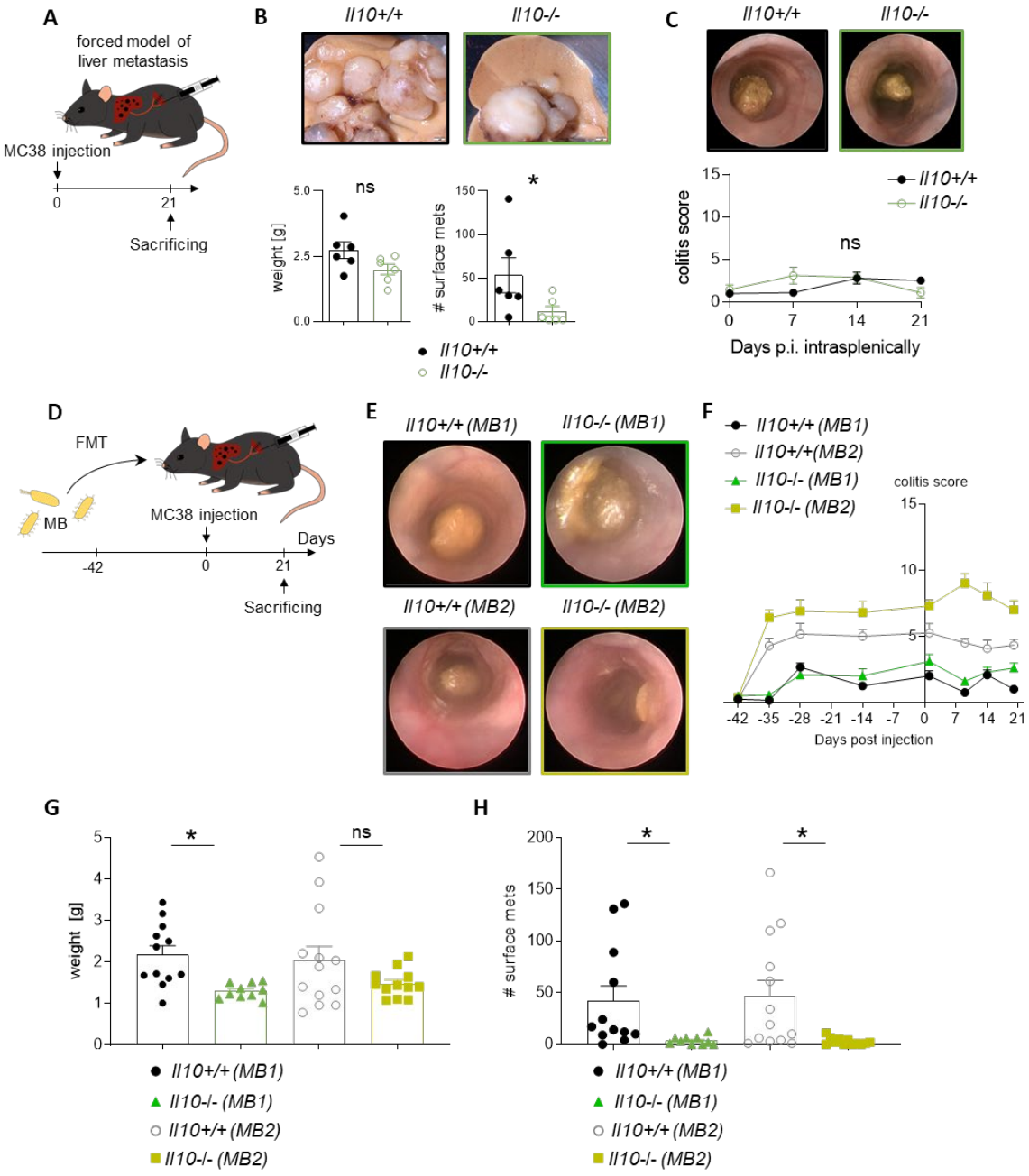

Fig. S2: The pathogenic role of IL-10 in liver metastasis formation is independent of colitis severity

(**A**) Schematic overview of the intrasplenic injection of MC38 cancer cells for forced liver metastasis induction in *Il10+/+* and *Il10-/-* littermates (n = 6 mice per group). (**B**) Representative pictures of liver metastasis, as well as analysis of liver weight and number of liver metastases. (**C**) Representative endoscopic view on day 21 and colitis score at different time points during liver metastasis formation. (**D**) Schematic overview of the i.s. injection of MC38 cancer cells for forced liver metastasis induction using *Il10+/+* and *Il10-/-* littermates following fecal microbiome (MB) transplant (*MB1, MB2*) (n ≥ 10 mice per group). (**E**) Representative endoscopic view of colon on day 21 post injection (i.s.) and (**F**) Colitis severity score at different time points during the whole

procedure. Livers were harvested and (**G**) liver weight as well as (**H**) number of microscopic liver metastases were analyzed. Scale bar: 2 mm. Data are presented as mean ± SEM. Non-significant (ns): $p > 0.05$; *: $p \leq 0.05$; **: $p < 0.01$, as calculated by Mann-Whitney *U* test or by one-way ANOVA with Bonferroni post hoc tests. FMT: fecal microbiome transfer.

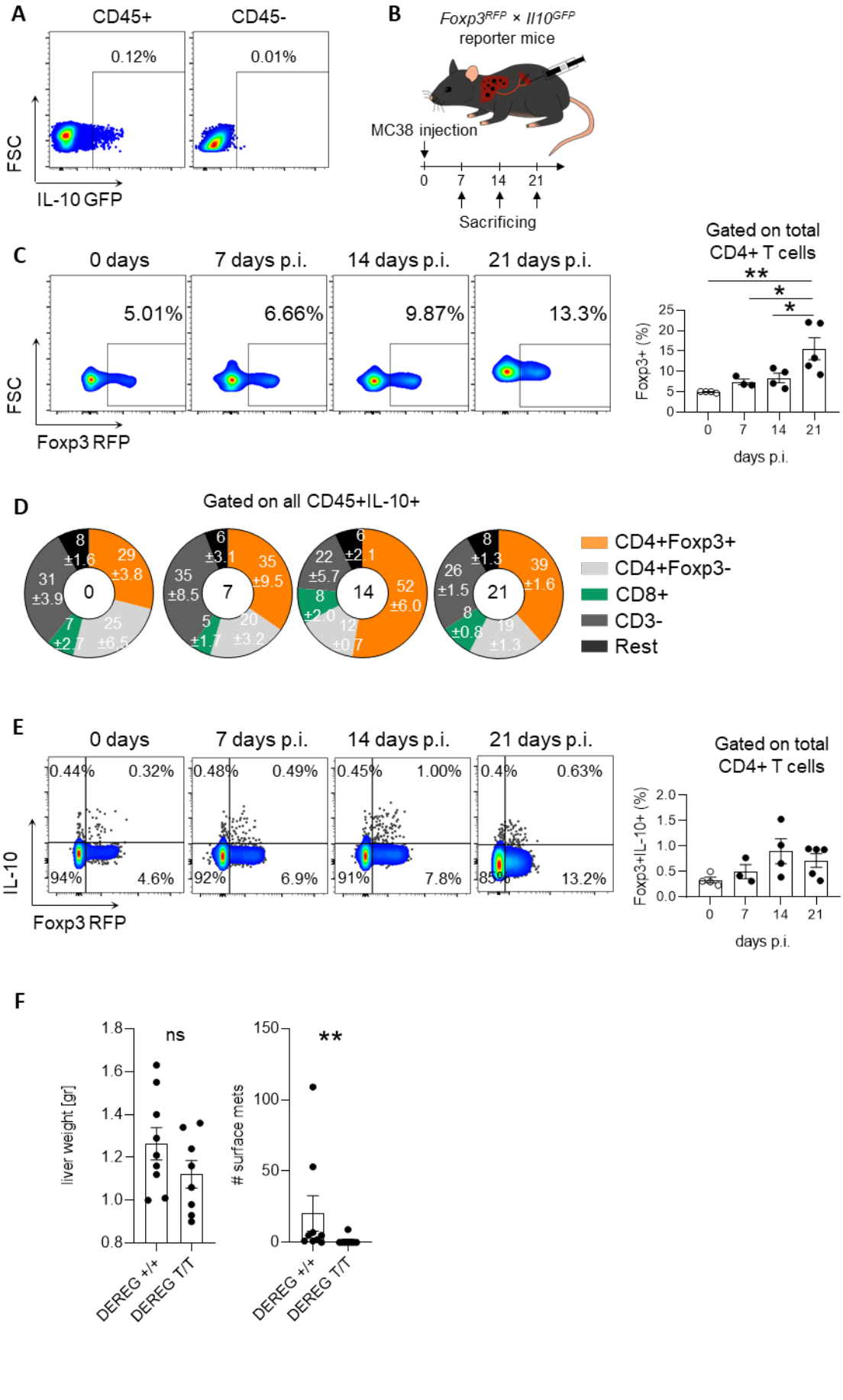
A
CD45+
CD45-
0.12%
0.01%
FSC
IL-10 GFP
B
Foxp3RFP × Il10GFP
reporter mice
MC38 injection
0
7
14
21
Sacrificing
C
0 days
7 days p.i.
14 days p.i.
21 days p.i.
5.01%
6.66%
9.87%
13.3%
FSC
Foxp3 RFP
Gated on total
CD4+ T cells
Foxp3+ (%)
days p.i.
D
Gated on all CD45+IL-10+
CD4+Foxp3+
CD4+Foxp3-
CD8+
CD3-
Rest
E
0 days
7 days p.i.
14 days p.i.
21 days p.i.
0.44%
0.32%
94%
4.6%
0.48%
0.49%
92%
6.9%
0.45%
1.00%
91%
7.8%
0.4%
0.63%
13.2%
IL-10
Foxp3 RFP
Gated on total
CD4+ T cells
Foxp3+IL-10+ (%)
days p.i.
F
ns
**
liver weight [gr]
surface mets
DEREG +/+
DEREG T/T

Fig. S3: Treg expansion together with a dynamic IL-10 increase are observed during liver metastasis formation

(**A**) IL-10 expression in hematopoietic and nonhematopoietic cells of a healthy mouse liver. (**B**) *Foxp3*^{RFP};*Il10*^{GFP} reporter mice received MC38 colon cancer cells i.s. and were sacrificed at the indicated time points (n ≥ 3 mice per group). (**C**) Frequency of Tregs within CD4+ T cells along metastasis formation. (**D**) General distribution of CD45+IL-10+ cells at the indicated timepoints. (**E**) IL-10 producing Tregs along metastasis formation. (**F**) *Wild type* and *DEREG* mice received i.s. of MC38 cells and livers were harvested in 21 days post injection. Liver weight (left) and number of liver metastasis (right) in mice with Treg depletion and their controls. Data are presented as mean ± SEM. Non-significant (ns): $p > 0.05$; *: $p \leq 0.05$; **: $p < 0.01$; ***: $p < 0.001$, as calculated by one-way ANOVA with Bonferroni post hoc tests.

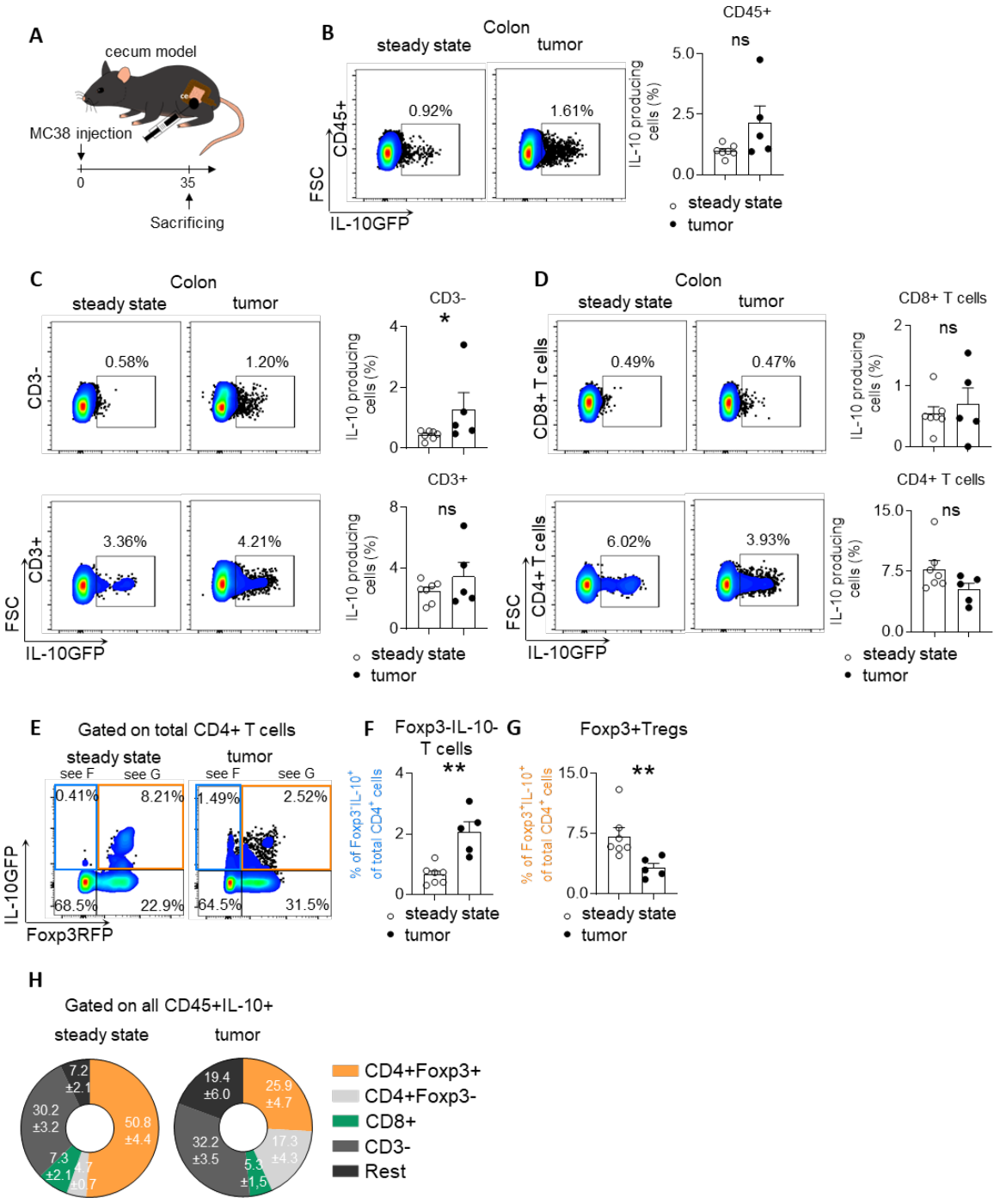

Fig. S4: Innate cells are the major source of IL-10 producing cells in CRC

(**A**) Schematic overview of the intracaecal injection of MC38 cancer cells for CRC induction in *Foxp3*^{RFP};*Il10*^{GFP} reporter mice (n ≥ 5 mice per group). Immune cells from cecum were then isolated and stained for flow cytometry 35 days post injection. The frequency of IL-10+ cells in the fraction of (**B**) CD45+ cells, (**C**) CD3- and T cells, and in (**D**) CD8+ T cells and CD4+ T cells was analyzed. (**E**) IL-10 expression in (**F**) Foxp3- IL-10+ T cells and (**G**) Foxp3+Tregs. (**H**) General distribution of all IL-10 producing CD45+ cells in healthy cecum and cecum tumor. Data are presented as mean ± SEM. Non-significant (ns): $p > 0.05$; *: $p \leq 0.05$; **: $p < 0.01$; ***: $p < 0.001$, as calculated by Mann-Whitney *U* test.

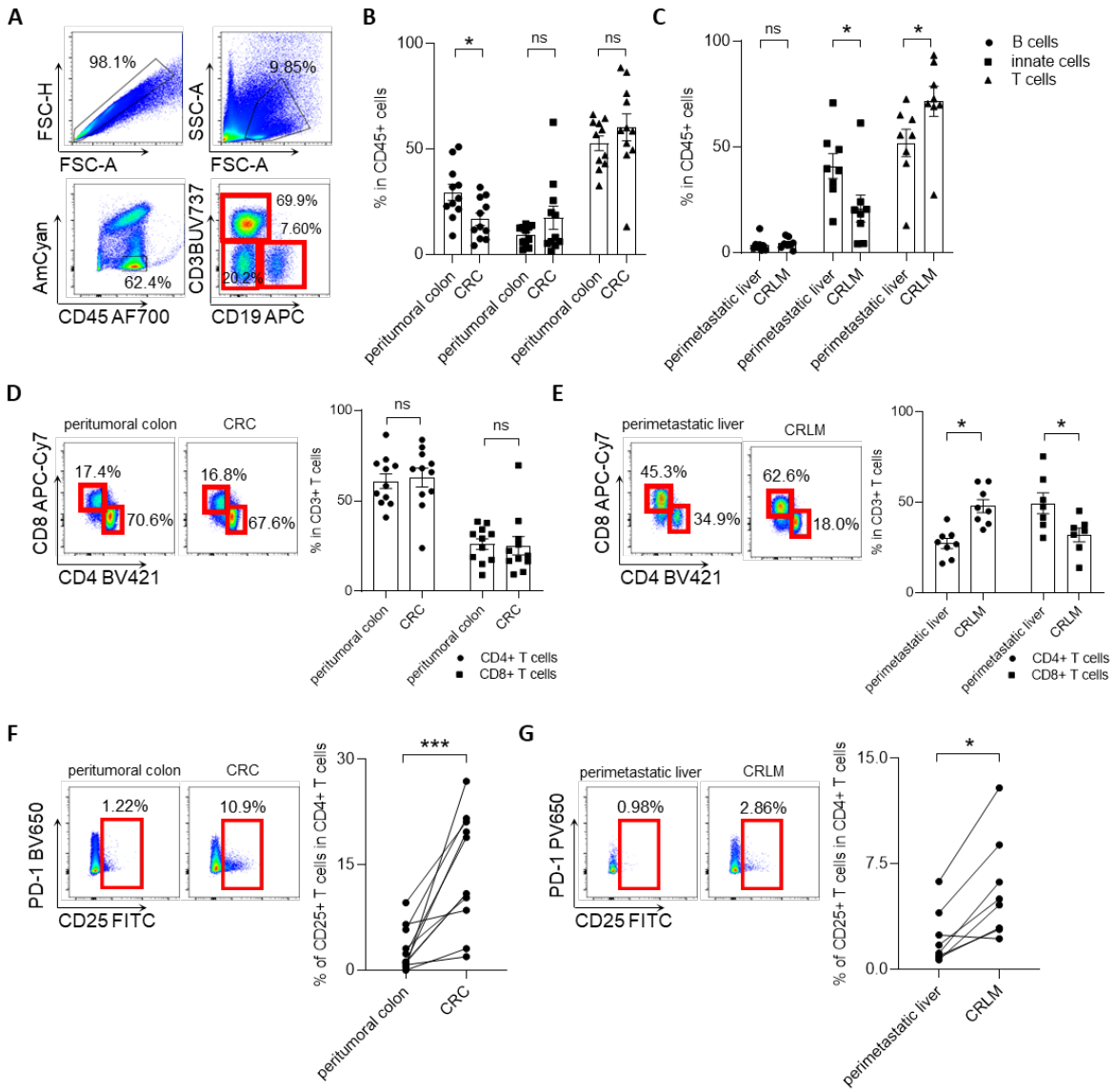

Fig. S5: Different immune cell compositions in CRC and CRLM. Immune cells were isolated from human CRC and CRLM, and subsequently stained for flow cytometry. (**A**) Gating strategy and analysis for B cells, innate cells and T cells in (**B**) CRC and (**C**) CRLM. (**D, E**) Representative FACS plots and analysis of CD4+ and CD8+ T cells in (D) CRC and (E) CRLM. (**F, G**) Representative FACS plots and analysis of CD4+CD25+ T cells in (D) CRC and (E) CRLM. Data are presented as mean ± SEM. Non-significant (ns): $p > 0.05$; *: $p \leq 0.05$; **: $p < 0.01$; ***: $p < 0.001$, as calculated by Mann-Whitney *U* test.

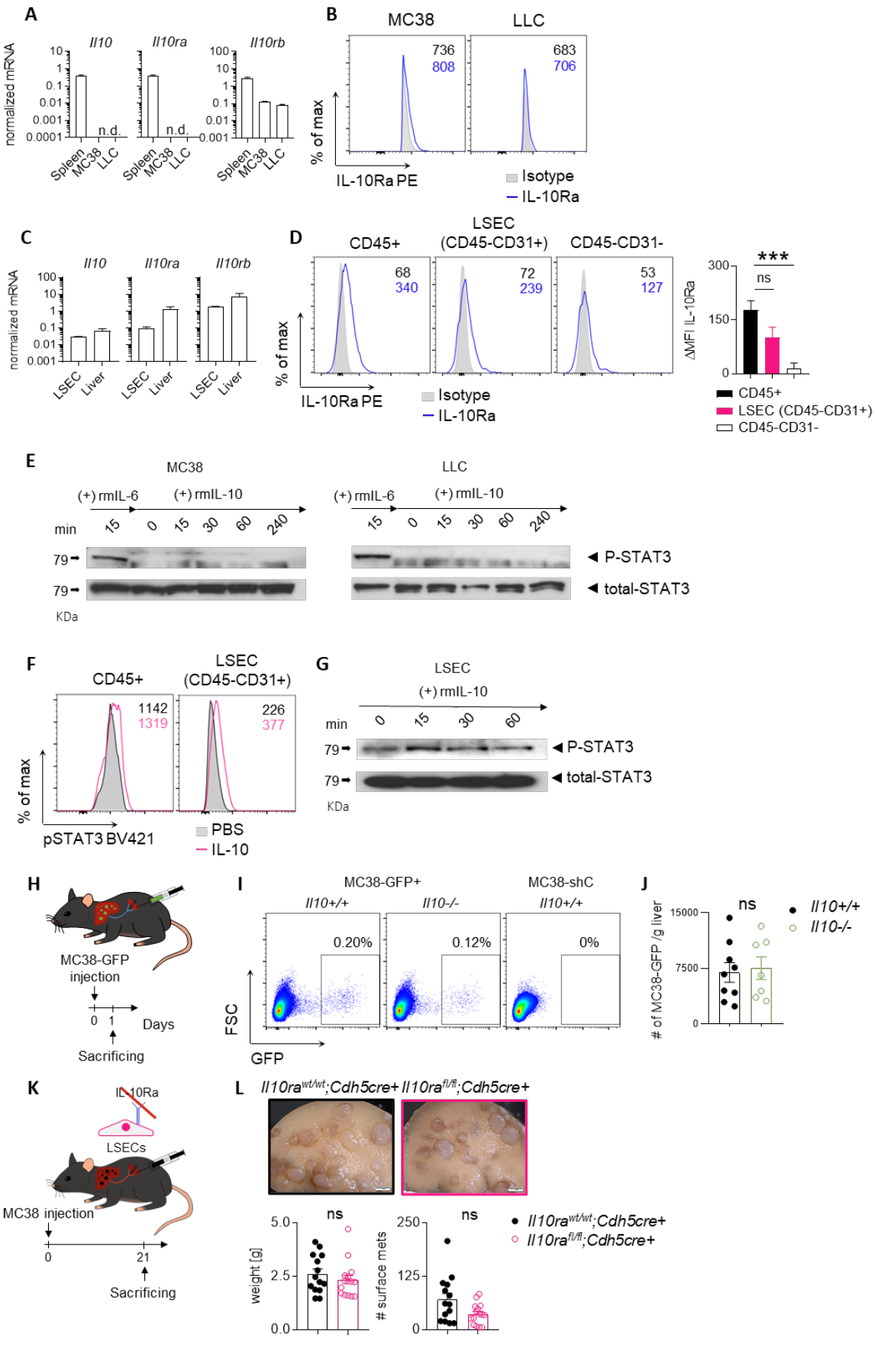
A
Il10
Il10ra
Il10rb
normalized mRNA
n.d.
Spleen
MC38
LLC
B
MC38
LLC
736
808
683
706
% of max
IL-10Ra PE
Isotype
IL-10Ra
C
Il10
Il10ra
Il10rb
normalized mRNA
LSEC
Liver
D
CD45+
LSEC (CD45-CD31+)
CD45-CD31-
68
340
72
239
53
127
% of max
IL-10Ra PE
Isotype
IL-10Ra
ΔMFI IL-10Ra
***
ns
CD45+
LSEC (CD45-CD31+)
CD45-CD31-
E
MC38
LLC
(+) rmIL-6
(+) rmIL-10
min
15
0
15
30
60
240
79
P-STAT3
total-STAT3
KDa
F
CD45+
LSEC (CD45-CD31+)
1142
1319
226
377
% of max
pSTAT3 BV421
PBS
IL-10
G
LSEC
(+) rmIL-10
min
0
15
30
60
79
P-STAT3
total-STAT3
KDa
H
MC38-GFP
injection
0
1
Days
Sacrificing
I
MC38-GFP+
MC38-shC
Il10+/+
Il10-/-
Il10+/+
0.20%
0.12%
0%
FSC
GFP
J
ns
Il10+/+
Il10-/-
# of MC38-GFP /g liver
15000
7500
0
K
IL-10Ra
LSECs
MC38 injection
0
21
Sacrificing
L
Il10ra^wt/wt;Cdh5cre+
Il10ra^fl/fl;Cdh5cre+
ns
weight [g]
5.0
2.5
0.0
ns
surface mets
250
125
0
Il10ra^wt/wt;Cdh5cre+
Il10ra^fl/fl;Cdh5cre+

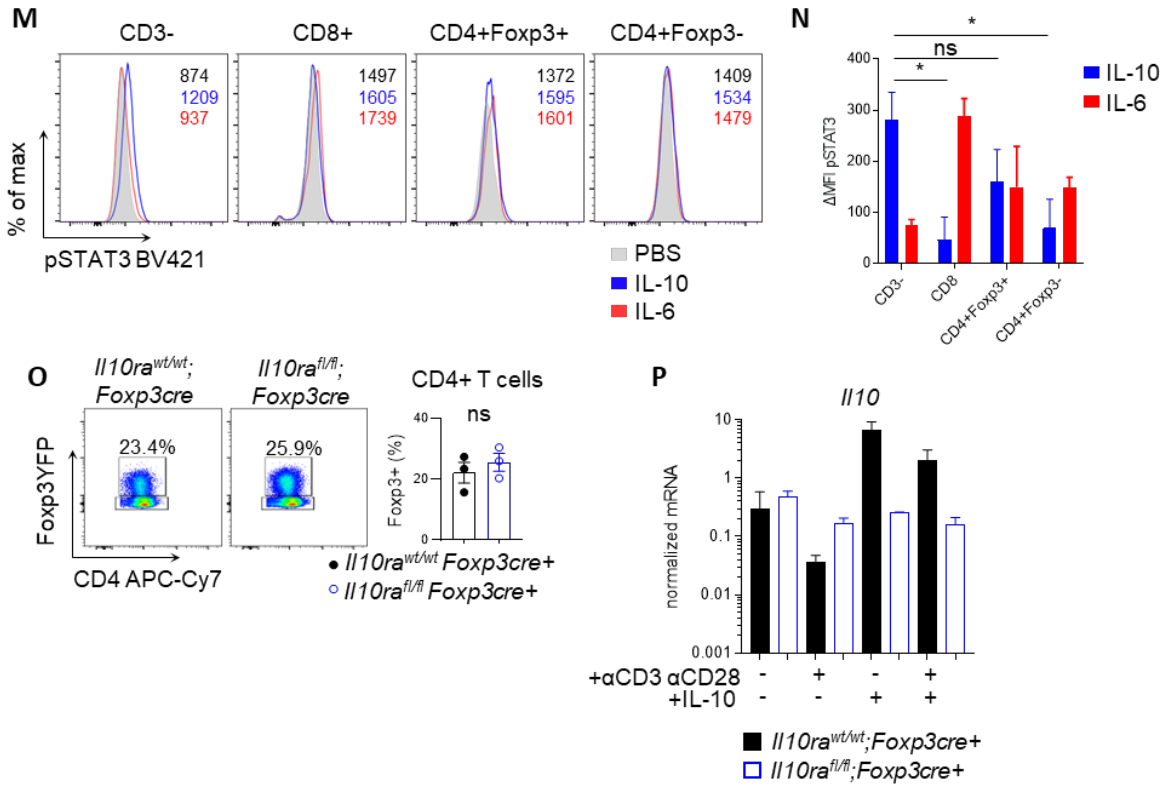

Fig. S6: IL-10 signaling in cancer cells and LSECs does not affect liver metastasis formation

(**A**) mRNA expression of the IL-10 and IL-10 receptor complex in MC38 and LLC cancer cells. (**B**) MFI of the IL-10Ra expression in MC38 and LLC cancer cells measured using flow cytometry. (**C**) mRNA expression of IL-10 and IL-10 receptor complex in total liver and LSECs isolated from *Wt* mice. (**D**) Quantification (ΔMFI) of IL-10Ra expression in total immune cells, LSECs and the rest of the cells isolated from *Wt* murine liver. (**E**) Phosphorylation of STAT3 in MC38 and LLC cancer cells upon *in vitro* IL-6 (10 ng/µl) or IL-10 (10 ng/µl) stimulation at indicated time points measured using Western Blot. (**F, G**) Phosphorylation of STAT3 in *Wt* LSECs after *in vitro* IL-10 stimulation (10 ng/µl) measured using (F) flow cytometry (after a 60-minute stimulation) or (G) Western blot (at indicated timepoints). (**H**) MC38-GFP cancer cells were intrasplenically injected into *Il10+/+* and *Il10-/-* littermates (n ≥ 7 mice per group). (**I**) Representative FACS-plot of extravasated MC38-GFP cells and (**J**) the number of extravasated MC38-GFP cells. (**K**) MC38 colon cancer cells were i.s. injected into mice with LSECs-specific IL-10Ra deletion and their littermate controls (n ≥ 12 mice per group). (**L**) Representative images, liver weight as well as number of liver metastasis were analyzed. (**M**) Representative FACS plot and (**N**) ΔMFI quantification of pSTAT3 staining in hepatic immune cells isolated from Wt mice upon IL-10 (10 ng/µl) or IL-6 (10 ng/µl) stimulation *in vitro*. (**O**) Hepatic Treg frequency within CD4+ T cells and (**P**) *Il10* level measured using qPCR upon IL-10 and/or antiCD3/CD28 stimulation *in vitro*. Scale bar: 2 mm. Data are presented as mean ± SEM. Non-significant (ns): $p > 0.05$; ***: $p < 0.001$, as calculated by Mann-Whitney *U* test or one-way ANOVA (Bonferroni) with Bonferroni post hoc tests. LSECs: liver sinusoidal endothelial cells.

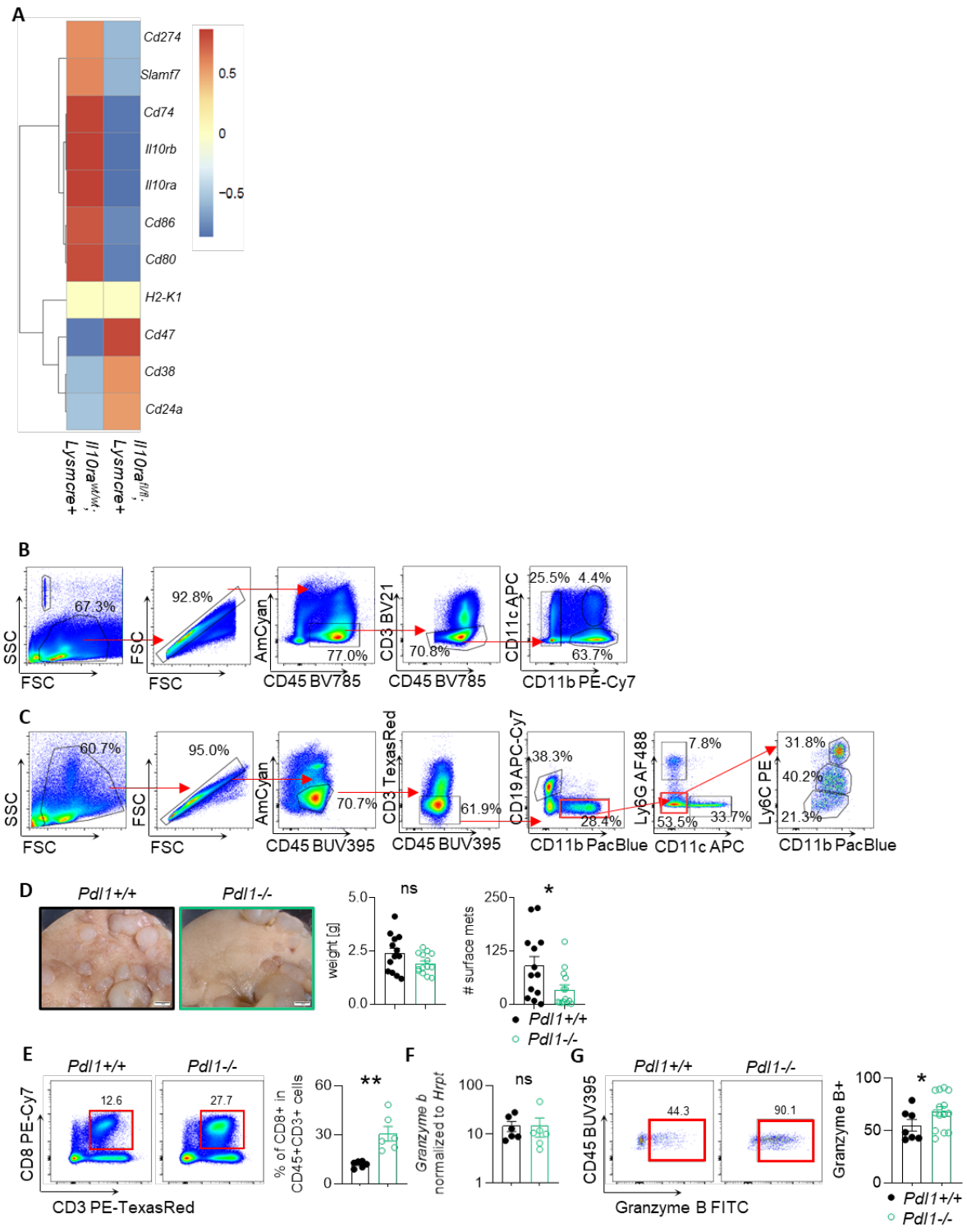

Fig. S7: PD-L1 deficiency enhances antitumor immunity of CD8+ T cells and reduces liver metastasis

(**A**) Bulk sequencing analysis on CD11b+ cells. (**B**) Gating strategy for Figure 6B. (**C**) Gating strategy for Figure 6C. (**D** to **G**) *Pdl1+/+* and *Pdl1-/-* mice were i.s. injected MC38 cancer cells (n ≥ 12 mice per group). (**D**) Livers were harvested 21 days post injection and metastatic burden was assessed. (**E**) 14 days post injection, representative FACS-plot and the frequency of hepatic CD8+ T cells, as well as

granzyme B level in CD8+ cells (**F**) before and (**G**) after coculture with MC38 cells *in vitro.* n ≥ 5 mice per group. Scale bar: 2 mm. Data are presented as mean ± SEM. Non-significant (ns): $p > 0.05$; *: $p \leq 0.05$; **: $p < 0.01$; ***: $p < 0.001$, as calculated by Mann-Whitney *U* test.

Supplementary materials and methods

LSEC isolation

The mice were euthanized and liver perfusion was performed, first by flushing with PBS, and then with 5 mL 0.05% collagenase into the portal vein and vena cava. The liver was sliced into small pieces and digested with 1 mg/ml collagenase and 10 U/ml DNase at 37°C for 25 minutes in RPMI (10% FBS, 1% pen/strep), while shaking. The remaining liver was filtered through a 200-µm cell strainer and cell isolation was performed by centrifuging twice at 40 g for 4 minutes and once at 400 g for 20 minutes. An Optiprep (Sigma, Kawasaki, Japan) gradient was used to enrich LSECs from theliver. For isolating LSECs, MACS sorting with anti-CD146 magnetic antibodies was used according to the manufacturer's protocol. LSECs were cultured on collagen-coated plates for 5 days before stimulation.

Extravasation assay

To perform the extravasation assay, the forced liver metastasis model was used as described above. Here, the difference was the time of euthanization and modified cancer cells. MC38 cells with a green fluorescent protein (MC38-GFP) were used for injections, and livers were harvested after 24 h. The livers were cut, digested and smashed into single cell resolution as mentioned above. Then, the supernatant was collected twice after a 40 g centrifuge for 4 mins. Next, cells in 1:10 dilution were mixed with counting beads (Spherotech Inc) for flow cytometry. A mouse injected with MC38shC cells was used as a negative control.

Fecal microbiome transfer

Stool was collected either from *C57BL/6J* mice (MB1) or from *Rag-/-(Yale)* mice with a colitogenic microbiome (MB2) [1]. Dissolved stool in brain heart infusion medium (Millipore) was transplanted into the recipient mouse using a gavage needle.

Mouse colonoscopy

A colonoscopy was performed to determine the severity of the colitis. The degree of colitis (scale 0-15) was determined as published [2], where 0 represents no colitis and 15 represents severe colitis. The mice were under isoflurane anesthesia, and the colonoscopy (Karl Storz) was performed once a week. Colitis severity was scored by two blinded investigators.

Western Blot

Cells were lysed in lysis buffer on a plate, then scraped and centrifuged at 14,000 g for 5 min. The supernatant was transferred to a new tube. Protein concentration was assessed using the NanoDrop-instrument. Protein samples were equalized with water and Laemmli buffer (60 µg/sample) and heated to 95°C for 5 min. Protein samples were run on a 10% Tris/Glyicine/SDS-PAGE, subsequently transferred from the gel to a PVDF-membrane using wet-blot electrophoresis for 60 min at 400 mA. The blotted membrane was incubated with blocking buffer (5% milk in PBS-T) for 1 hour, followed

by an incubation with antibody solution (1:1000 dilution) overnight at 4°C. The membrane was washed and incubated with the HRP-conjugated secondary antibody (1:2000) for 1 h. After washing, the blot was developed with chemiluminescent HRP substrate for 5 min before placing a film on the membrane (dark room). The photo film was run through a developer and the ladder was carefully marked on the film.

Bulk sequencing

To generate sequencing libraries, 2 mg RNA from each sample was used according to the manufacturer of NEBNext UltraTM RNA Library Prep Kit for Illumina (New England Biolabs, Ipswich, MA, USA). cDNA libraries were subsequently sequenced on Illumina HiSEquation 2500 yielding ~15 million 50 bp single-end reads per sample. To assess the RNA quality, FastQC v. 0.11.5 was used [3]. Alignment to mouse genome draft GRCm38.84 was conducted using STAR v. 2.5.0 [4]. For visualization and hierarchical clustering, using the transcripts per million method was used to normalize the reads, but raw read counts were used for differential expression analysis using DESeq2 v. 1.14 [5].

[1] **Palm NW, de Zoete MR**, Cullen TW, Barry NA, Stefanowski J, Hao L, et al. Immunoglobulin A coating identifies colitogenic bacteria in inflammatory bowel disease. Cell 2014;158:1000-1010.
[2] Becker C, Fantini MC, Wirtz S, Nikolaev A, Kiesslich R, Lehr HA, et al. In vivo imaging of colitis and colon cancer development in mice using high resolution chromoendoscopy. Gut 2005;54:950-954.
[3] Bolger AM, Lohse M, Usadel B. Trimmomatic: a flexible trimmer for Illumina sequence data. Bioinformatics 2014;30:2114-2120.
[4] Dobin A, Davis CA, Schlesinger F, Drenkow J, Zaleski C, Jha S, et al. STAR: ultrafast universal RNA-seq aligner. Bioinformatics 2013;29:15-21.
[5] Li B, Dewey CN. RSEM: accurate transcript quantification from RNA-Seq data with or without a reference genome. BMC Bioinformatics 2011;12:323.

Table S1: Taqman probes and primer sequences utilized for this study

gene	company	taqman probe/primer name	sequence (5' → 3')
		IL-10fw	GCC TTC AGT ATA AAA GGG GGA CC
		IL-10rev	GTG GGT GCA GTT ATT GTC TTC CCG
Il10-/-	Eurofins Genomics	IL10 neo	CCT GCG TGC AAT CCA TCT TG
		IL10fl 932	CCA GCA TAG AGA GCT TGC ATT ACA
Il10flox/flox	Eurofins Genomics	IL10fl 933	GAG TCG GTT AGC AGT ATG TTG TCC AG
		Foxp3 KI (F) 936	AGG ATG TGA GGG ACT ACC TCC TGT A
		Foxp3 KI (Rev) 937	TCC TTC ACT CTG ATT CTG GCA ATT T
		Foxp3 wt (F)	CCT AGC CCC TAG TTC CAA CC
Foxp3cre+	Eurofins Genomics	Foxp3 wt (Rev)	AAG GTT CCA GTG CTG TTG CT
		LysM Wt	TA CAG TCG GCC AGG CTG AC
		LysM common	CTT GGG CTG CCA GAA TTT CTC
Lysmcre+	Eurofins Genomics	LysM Mut	CCC AGA AAT GCC AGA TTA CG
		RagWF	GAG GTT CCG CTA CGA CTC TG
		RagR	CCG GAC AAG TTT TTC ATC GT
Rag-/-(Yale)	Eurofins Genomics	RagMF	TGG ATG TGG AAT GTG TGC GAG
		GFP-3	AAG TCG TGC TGC TTC ATG TG
		GFP-5	ACG TAA ACG GCC ACA AGT TC
		IL10KOF	GTG TGT ATT GAG TCT GCT GGA C
		IL10KOR1	GTG TGG CCA GCC TTA GAA TAG
Il10eGFP	Eurofins Genomics	IL10KOR2	GGT TGC CTT GAC CAT CGA TG
		FIR1	CAA AAC CAA GAA AAG GTG GGC
		FIR2	GGA ATG CTC GTC AAG AAG ACA GG
Foxp3RFP	Eurofins Genomics	FIR3	CAT CTT GGA GAG TCG GTG TG
		YAK235	ACT GCT GTA TCC CCT CAT CT
Il10raflox/flox		YAK236	GTG AGC GGA GAT TTT AAC AG
		Cdh5-Cre Fw	GTC CAA TTT ACT GAC CGT ACA C
Cdh5cre+	Eurofins Genomics	Cdh5-Cre Rev	CTG TCA CTT GGT CGT GGC AGC
		17AyfpF	CAA GTG CAC CCA GCA CCA GCT GAT C
		17AyfpRwt	CTT AGT GGG TTA GTT TCA TCA CAG C
Il17acre+	Eurofins Genomics	17AyfpCreR	GCA GCA GGG TGT AGG CAA TGC
		Rosa26 Seq1	AAA GTC GCT CTG AGT TGT TAT
		Rosa26 Seq2	GCG AAG AGT TTG TCC TCA ACC
a26floxSTOPflox YFP	Eurofins Genomics	Rosa26 Seq3	GGA GCG GGA GAA ATG GAT ATG
		63PC3CreF	TTC CCG CAG AAC CTG AAG ATG TTC G
Cd11ccre+	Eurofins Genomics	64PC3CreR	GCC AGA TTA CGT ATA TCC TGG CAG
		B7H1 P2	ATT GAC TTT CAG CGT GAT TCG CTT GTA G
		B7H1 P3	TTC TAT CGC CTT CTT GAC GAG TTC TTC TG
		B7H1 P1	AGA ACG GGA GCT GGA CCT GCT TGC GTT AG
Pdl1-/-	Eurofins Genomics	B7H1 P2	ATT GAC TTT CAG CGT GAT TCG CTT GTA G
Hprt	Thermo Fisher Scientific	Mm03024075_m1	
Il10	Thermo Fisher Scientific	Mm00439614_m1	
Il10ra	Thermo Fisher Scientific	Mm00434151_m1	
Il10rb	Thermo Fisher Scientific	Mm00434157_m1	
Granzyme B	Thermo Fisher Scientific	Mm00442837_m1	

Table S2: Flow cytometry antibodies utilized for this study

Antibody	Fluorochrom	company	Cat#	Clone	RRID
CD45	BV785	Biolegend	103149	30-F11	AB_2564590
CD45	BUV395	BD	564279	30-F11	AB_2651134
CD3	BV421	Biolegend	100228	17A2	AB_2562553
CD3	PE-Dazzle	Biolegend	100246	17A2	AB_2565883
CD3	BV650	Biolegend	100229	17A2	AB_11204249
CD3	BUV395	BD	740268	17A2	AB_2687927
CD4	APC	Biolegend	100412	GK1.5	AB_312697
CD4	BUV737	BD	612761	GK1.5	AB_2870092
CD8	PE-Cy7	Biolegend	100722	53-6.7	AB_312761
IL-10Ra	PE	Biolegend	112706	1B1.3a	AB_313519
Isotype	PE	Biolegend	400408	RTK2071	AB_326514
pSTAT3	BV421	Biolegend	651010	13A3-1	AB_2572088
PD-L1	BV711	Biolegend	124319	10F.9G2	AB_2563619
PD-1	BV421	Biolegend	135218	29F.1A12	AB_2561447
CD11b	PacBlue	Biolegend	101224	M1/70	AB_755986
CD11c	APC	Biolegend	117312	N418	AB_389328
Ly6G	AF488	Biolegend	127625	1A8	AB_2561339
Ly6C	PE	Biolegend	560592	AL-21	None availiable
CD19	APC-Cy7	Biolegend	115530	6D5	AB_830707
Fixable Viability Dye eFluor 506	BV510	Invitrogen	65-0866-14	ıg doesnt target a spe	None availiable
PI	PE	Invitrogen	P1304MP	/	None availiable
Annexin	APC	Biolegend	640920	/	None availiable
TNFa	BV421	Biolegend	506328	MP6-XT22	AB_2562902
Granzym B	FITC	BioLegend	515403	GB11	AB_2114575